

ARTICLE TYPE

An hp -adaptive multi-element stochastic collocation method for surrogate modeling with information re-use

Armin Galetzka¹ | Dimitrios Loukrezis^{1,2,4} | Niklas Georg^{1,2,3} | Herbert De Gersem^{1,2} | Ulrich Römer³¹Institute for Accelerator Science and Electromagnetic Fields, TU Darmstadt, Darmstadt, Germany²Centre for Computational Engineering, TU Darmstadt, Darmstadt, Germany³Institut für Dynamik und Schwingungen, TU Braunschweig, Braunschweig, Germany⁴Technology, Siemens AG, Munich, Germany**Correspondence**

Armin Galetzka, Email: galetzka@temf.tu-darmstadt.de

Present Address

Schlossgartenstr. 8, 64289 Darmstadt, Germany

Funding Information

This research was supported by the German Research Foundation (DFG) via grants GRK 2128 (project number: 264883531) and TRR 361 (project number: 492661287)

Abstract

This paper introduces an hp -adaptive multi-element stochastic collocation method, which additionally allows to re-use existing model evaluations during either h - or p -refinement. The collocation method is based on weighted Leja nodes. After h -refinement, local interpolations are stabilized by adding Leja nodes on each newly created sub-element in a hierarchical manner. A dimension-adaptive algorithm is employed for local p -refinement. The suggested multi-element stochastic collocation method is employed in the context of forward and inverse uncertainty quantification to handle non-smooth or strongly localised response surfaces. Comparisons against existing multi-element collocation schemes and other competing methods in five different test cases verify the advantages of the suggested method in terms of accuracy versus computational cost.

KEYWORDS:

hp -adaptivity; multi-element approximation; stochastic collocation; surrogate modeling; uncertainty quantification

1 | INTRODUCTION

Prediction and optimization with computational models is now routinely carried out in many fields of science and engineering. For instance, reliable predictions require the propagation and quantification of uncertainties¹ related to parameter calibration from noisy and limited data. The so-called non-intrusive approach is widely adopted, where computer codes are treated as black box functions from model parameters to quantities of interest. In this way, restructuring and modifying complex software is avoided. Exemplarily, in forward uncertainty quantification (UQ)², also referred to as uncertainty propagation, non-intrusive methods evaluate the model at selected points of the input vector, which are generated according to the underlying probability distribution. Similarly, in inverse UQ³, repeated model evaluations are required to build the likelihood function at individual elements of a Markov chain.

Even when large computational resources are available, such multi-query simulations with complex models present a widely acknowledged challenge. This fact has led to significant research efforts in the area of surrogate modeling^{4,5}, for example, by means of neural networks⁶, Gaussian processes⁷, or polynomial chaos expansions (PCEs)⁸. Surrogate modeling can be carried out efficiently if the response function is sufficiently smooth and if the function varies moderately over the parameter space. However, there exist many examples in engineering and mechanics where the response is discontinuous or exhibits strong variations and sharp transitions⁹. In this case, most surrogate modeling techniques become too computationally expensive or altogether unreliable, thus, Monte Carlo methods are usually preferred. Nevertheless, an efficient sampling scheme is adapted to a specific simulation task and the computed model responses cannot be re-used in a different context. This is a major bottleneck

of pure sampling approaches and a strong motivation to develop flexible and robust surrogate models, which can be applied even if the model response is non-smooth.

The family of multi-element methods^{10–14} presents a class of approximation techniques which have been successfully applied in the UQ context for addressing non-smooth stochastic response functions. In a multi-element method, the parameter space is decomposed into subdomains referred to as *elements*, where local polynomial basis functions are used. Here, we focus on the non-intrusive multi-element stochastic collocation method for forward and inverse UQ. Although several proposals for multi-element collocation exist^{14–20}, a number of challenges remain to be addressed. Most notably, computational efficiency considerations require to limit the number of collocation points, which is problematic since existing points do not necessarily fit to a collocation pattern once the subdomains in the parameter space are refined. Another challenge is to efficiently implement dimension adaptivity to avoid using large tensor grids in the parameter domain. To that end, multi-element collocation methods can greatly benefit from *hp*-adaptivity concepts, which are well established in the finite element literature²¹. Therein, adaptive *h*-refinement, also referred to as *h*-adaptivity, refers to the adaptive decomposition of the computational domain into subdomains where local polynomial approximations are developed, while *p*-adaptivity refers to increasing the local polynomial degree within a subdomain. These concepts have already been successfully applied for UQ purposes in the context of the stochastic Galerkin method²². However, multi-element collocation methods so far rely on *h*-adaptivity only.

In this work, we present a new *hp*-adaptive multi-element stochastic collocation method, which re-uses existing model evaluations during both *h*- and *p*-refinement. The main ingredient of the method is the use of weighted Leja collocation points²³. A given sequence of collocation points can be stabilized by adding additional Leja points in a greedy way. Hence, on each element the collocation scheme can be stabilized by enriching the collocation set. This information re-use improves the efficiency of the overall scheme, which we demonstrate with several examples, also in comparison to existing approaches. Regarding *p*-adaptivity, we rely on the nestedness and granularity of Leja points to realize dimension-adaptive collocation^{24,25} on each element, where the polynomial order in each dimension can be increased one-by-one. Our approach contributes to the growing literature on adaptive surrogate models in the field of UQ and can be used both in forward and inverse UQ analysis, which we illustrate in the numerical examples. Therein, we restrict ourselves to problems with a relatively low dimensionality of random inputs, due to the fact that the complexity of the method scales with $\mathcal{O}(2^N)$, where the exponent refers to the number of random inputs and the base to the subdomain splitting which is performed in the *h*-refinement step. This bottleneck is known to affect most, if not all, multi-element methods suggested in the literature^{26,27}.

The remaining of this paper is structured as follows. In Section 2, we introduce the notation and some necessary preliminaries on stochastic collocation methods. Section 3 is concerned with stochastic collocation on Leja grids, based either on hierarchical interpolation or on PCE. In Section 4, we introduce our novel *hp*-adaptive multi-element stochastic method based on Leja grids, which additionally allows for re-using model evaluations after either *h*- or *p*-refinement. Numerical results showcasing the advantages of the proposed multi-element stochastic collocation method are reported in Section 5. Finally, conclusions are drawn in Section 6.

2 | PRELIMINARIES AND NOTATION

In this section, we introduce the notation and the stochastic setting in particular. We also present the main ideas of stochastic collocation as a surrogate approach for forward and inverse problems. Details of the collocation method are postponed until Section 3.

2.1 | Stochastic surrogate modeling

We consider a parameter-dependent model that receives as input a parameter vector and estimates an output, represented through the map

$$g : \mathbf{x} \mapsto g(\mathbf{x}). \quad (1)$$

In (1), $\mathbf{x} \in \mathbb{R}^N$ denotes the input parameter vector and $g(\mathbf{x}) \in \mathbb{R}^{N_{\text{out}}}$ the model evaluation for the given input parameters. In forward analyses, e.g. in the context of uncertainty propagation, $g(\mathbf{x})$ is typically called the quantity of interest (QoI). In inverse problem settings, $g(\mathbf{x})$ represents the map from parameters to observations or the likelihood function. In cases where an evaluation $g(\mathbf{x})$ is computationally expensive, e.g. the model in question is a high-fidelity numerical solver, an inexpensive

approximation $\tilde{g}(\mathbf{x}) \approx g(\mathbf{x})$ that can reliably replace the original model is often desirable. This is particularly true for multi-query tasks in UQ, optimization, or design space exploration. We refer to such an approximation as a *surrogate model*.

In the context of this work, the inputs \mathbf{x} are assumed to be realizations of independent random variables (RVs) $X_n, n = 1, 2, \dots, N$, which are collected in the multivariate RV $\mathbf{X} = (X_1, X_2, \dots, X_N)^\top$, also referred to as a random vector. The random vector \mathbf{X} is defined on the probability space (Θ, Σ, P) , where Θ denotes the sample space, Σ the sigma algebra of events, and $P : \Sigma \rightarrow [0, 1]$ the probability measure. We further introduce the image space $\Xi \subset \mathbb{R}^N$ such that $\mathbf{X} : \Theta \rightarrow \Xi$, equivalently, $\mathbf{X}(\theta) = \mathbf{x}$ with $\theta \in \Theta$ and $\mathbf{x} \in \Xi$, as well as the probability density function (PDF) $\pi_{\mathbf{X}}(\mathbf{x}) : \Xi \rightarrow \mathbb{R}_{\geq 0}$. Note that the notation differentiates between a random vector \mathbf{X} and a realization $\mathbf{x} = \mathbf{X}(\theta)$. Recalling that the individual RVs $X_n, n = 1, \dots, N$, are mutually independent, it holds that $\pi_{\mathbf{X}}(\mathbf{x}) = \prod_{n=1}^N \pi_{X_n}(x_n)$ and $\Xi = \Xi_1 \times \dots \times \Xi_N$, where $\pi_{X_n}(x_n)$ and Ξ_n refer to the marginal (univariate) PDFs and image spaces, respectively. Then, the model output is a RV dependent on the input random vector \mathbf{X} . Note that the model itself remains purely deterministic, i.e. the uncertainty in the model output is caused only due to the random input parameters. Accordingly, a RV realization \mathbf{x} corresponds to an estimation $g(\mathbf{x})$ of fixed value.

2.2 | Stochastic collocation methods

The term *stochastic collocation*^{28,29} refers to a class of sampling-based methods where a model g is evaluated (sampled) on a set of so-called *collocation points* $\mathcal{X} = \{\mathbf{x}_j\}_{j=1}^J$. The pairs of collocation points and corresponding model evaluations $\{\mathbf{x}_j, g(\mathbf{x}_j)\}_{j=1}^J$ are then utilized to compute a surrogate model $\tilde{g}(\mathbf{x}) \approx g(\mathbf{x})$, which typically takes the form

$$\tilde{g}(\mathbf{x}) = \sum_{i=1}^I \beta_i B_i(\mathbf{x}), \quad (2)$$

where $\beta_i \in \mathbb{R}^{N_{\text{out}}}$ are coefficients, B_i appropriately chosen basis functions, and I the size of the basis. In a collocation approach, the coefficients are determined based on the condition

$$g(\mathbf{x}_j) = \tilde{g}(\mathbf{x}_j), \quad \forall j = 1, \dots, J, \quad (3)$$

where $I = J$, resulting in a linear system of equations for β_i . The well-known Lagrange basis even results in $\beta_i = g(\mathbf{x}_i)$. A major challenge for surrogate models in the form (2) is the rapidly growing size of the basis when the input dimension is large. In this case, constructing a sparse basis has often proven to be useful^{28,30}. Even in case of sparse approximation, the construction of the polynomial basis relies on tensor product polynomials, hence, the one-dimensional case serves as the starting point. This approach is adopted in Section 3.

Before discussing details of the *hp*-adaptive collocation approach, we briefly outline the role of surrogate models in inverse and forward UQ. In forward UQ, the goal is to compute moments or a distribution function of the QoI. This can be achieved, either by sampling the inexpensive surrogate model, or by choosing a suitable basis from which the sought quantities can be readily obtained. The polynomial chaos basis, for instance, allows to infer the moments directly from the basis coefficients without involving any additional sampling routine^{8,31}. In inverse UQ, an important object is the likelihood function which, in the common case of Gaussian noise, reads

$$L(\mathbf{x}|\mathbf{b}) = \exp\left(-\frac{1}{2} \|\mathbf{b} - \mathcal{G}(\mathbf{x})\|_{\Sigma^{-1}}\right), \quad (4)$$

where $\mathbf{b} \in \mathbb{R}^D$ denotes the observation vector and Σ the noise covariance matrix. Then, $\mathcal{G} : \mathbb{R}^N \rightarrow \mathbb{R}^D$ represents the nonlinear relationship between input parameters and observations. In (4), the model-data mismatch is measured in the discrete Euclidean norm, weighted with the inverse covariance matrix. When running a Markov chain Monte Carlo analysis, the likelihood function and hence, the model included in \mathcal{G} , needs to be evaluated for each entry of the chain. To reduce the large computational workload, a surrogate model $\tilde{g}(\mathbf{x}) \approx g(\mathbf{x}) = \mathcal{G}(\mathbf{x})$ can be employed³². A more recent approach constructs a surrogate for the likelihood as $\tilde{g}(\mathbf{x}) \approx g(\mathbf{x}) = L(\mathbf{x}|\mathbf{b})$, which allows to avoid any sampling-based analysis³³. However, in the large data - small noise regime, the likelihood function is highly concentrated and global surrogate modeling is difficult. One possible remedy to this problem is to use the spectral stochastic embedding (SSE) method³³. We will show in Section 5, that our multi-element stochastic collocation method is also capable of handling such highly concentrated likelihood functions.

3 | STOCHASTIC COLLOCATION ON LEJA GRIDS

Next, we elaborate on the concept of hierarchical Leja collocation in one- and multiple dimensions and its relation to polynomial chaos surrogates.

3.1 | Leja sequences

In their original form, Leja sequences³⁴ are sequences of points $\{x_i\}_{i \geq 0}$, $x_i \in [-1, 1]$, $\forall i \geq 0$, where the initial point x_0 is chosen arbitrarily within $[-1, 1]$ and the remaining points are computed by solving the optimization problem

$$x_i = \operatorname{argmax}_{x \in [-1, 1]} \prod_{k=0}^{i-1} |x - x_k|. \quad (5)$$

A point sequence produced by formula (5) is an *unweighted* Leja sequence. *Weighted* Leja sequences are constructed by incorporating a continuous and positive weight function in the definition of Leja sequences²³. Assuming that the weight function is a PDF $\pi_X(x) : \Xi \rightarrow \mathbb{R}_{\geq 0}$, the points of the corresponding weighted Leja sequence are given as

$$x_i = \operatorname{argmax}_{x \in \Xi} \sqrt{\pi_X(x)} \prod_{k=0}^{i-1} |x - x_k|, \quad (6)$$

where again the initial Leja point x_0 is chosen arbitrarily within the image space Ξ .

Leja points are known to perform well when employed as interpolation or quadrature nodes^{25,35–38}. With respect to interpolation in particular, the Lebesgue constant of Leja sequence based interpolation grids is known to grow subexponentially^{39–41}, thus resulting in comparatively stable interpolations. Additionally, interpolation and quadrature grids with respect to any continuous PDF can be constructed by using weighted Leja sequences^{42–45}. Moreover, due to the fact that Leja sequences are by definition nested, i.e. $\{x_i\}_{i=0}^j \subset \{x_i\}_{i=0}^{j+1}$, they allow for re-using readily available Leja points and model evaluations on those points in case the sequence is further expanded. Due to the nestedness property, Leja points are natural candidates for constructing sparse interpolation or quadrature grids^{24,46–49}. Note that nested interpolation and quadrature grids can be obtained with other types of nodes, such as Clenshaw-Curtis⁵⁰. However, Leja sequences have the additional attractive feature of retaining the nestedness property even if a single point is added to the sequence, thus allowing for arbitrary grid granularity. Nestedness and grid granularity become additionally important considering efficient h -refinement, as discussed in Section 4.

3.2 | Hierarchical interpolation on Leja grids

In interpolation based stochastic collocation methods^{28–30}, the surrogate model $\tilde{g}(\mathbf{x}) \approx g(\mathbf{x})$ is a global polynomial approximation computed by means of interpolation. For simplicity, in the following we assume a scalar model output $g(\mathbf{x}) \in \mathbb{R}$, however, the extension to vector-valued outputs is straightforward by a component-wise application of the method.

Considering a model $g(\mathbf{x})$ dependent on a single parameter and an interpolation grid $\mathcal{X}_j = \{x_i\}_{i=0}^j$, a Lagrange interpolation based approximation is given as

$$\tilde{g}(\mathbf{x}) = \mathcal{I}_j[g](\mathbf{x}) = \sum_{i=0}^j g(x_i) l_i^j(\mathbf{x}), \quad (7)$$

where l_i^j are Lagrange polynomials of degree j , defined as

$$l_i^j(\mathbf{x}) = \prod_{k=0, k \neq i}^j \frac{x - x_k}{x_i - x_k}, \quad l^0 = 1. \quad (8)$$

Assuming that the interpolation grid \mathcal{X}_j coincides with a Leja sequence, a sequence of nested grids can be defined, such that $\mathcal{X}_0 = \{x_0\} \subset \mathcal{X}_1 = \{x_0, x_1\} \subset \dots \subset \mathcal{X}_j = \{x_0, x_1, \dots, x_j\}$, where each grid defines an interpolation operator $\mathcal{I}_i[g](\mathbf{x})$, $i = 0, 1, \dots, j$. Then, replacing the Lagrange polynomials with the hierarchical polynomials²⁴

$$h^i(\mathbf{x}) = \prod_{k=0}^{i-1} \frac{x - x_k}{x_i - x_k}, \quad h^0(\mathbf{x}) = 1, \quad (9)$$

of polynomial degree i , $i = 0, 1, \dots, j$, a sequential interpolation formula can be derived, such that

$$\tilde{g}(x) = \mathcal{I}_j[g](x) = \sum_{i=0}^j s_i h^i(x) = \sum_{i=0}^j (g(x_i) - \mathcal{I}_{i-1}[g](x_i)) h^i(x), \quad (10)$$

where the coefficients s_i are called the hierarchical surpluses⁵¹. Note that \mathcal{I}_{-1} is a null operator, i.e. $\mathcal{I}_{-1}[g](x) = 0$, accordingly, $s_0 = g(x_0)$. We shall refer to the interpolation format (10) as *hierarchical* interpolation.

The interpolation formats (7) and (10) are in fact equivalent, as the interpolating polynomial is unique for a given interpolation grid irrespective of the choice of the polynomial basis⁵². The hierarchical representation (10) offers the advantage that, if the Leja sequence based interpolation grid is expanded with new nodes, the already computed basis polynomials remain unchanged. Accordingly, each hierarchical polynomial h^i , $i = 0, 1, \dots, j$, has a degree equal to i which is unique. The property of degree uniqueness per basis polynomial significantly simplifies transformations to other polynomial bases with the same property, e.g. the orthonormal PCE basis discussed in section 3.3. Irrespective of the choice of basis polynomials, a crucial advantage of using Leja sequences as interpolation grids is that the readily available model evaluations $g(x_i)$, $x_i \in \mathcal{X}_j$, $i = 0, 1, \dots, j$, that are used to construct the interpolation $\mathcal{I}_j[g](x)$, can be re-used for the interpolation $\mathcal{I}_{j+1}[g](x)$, due to the fact that $\mathcal{X}_j \subset \mathcal{X}_{j+1}$. Accordingly, the model needs to be evaluated only on the new Leja point x_{j+1} , where $\{x_{j+1}\} = \mathcal{X}_{j+1} \setminus \mathcal{X}_j$.

Moving to an N -variate model $g(\mathbf{x})$, we introduce a multi-index notation such that a multi-index $\mathbf{j} = (j_1, \dots, j_N)$ can be uniquely associated with the multivariate Leja node $\mathbf{x}_j = (x_{1,j_1}, \dots, x_{N,j_N})$, the multivariate hierarchical polynomial

$$H_{\mathbf{j}}(\mathbf{x}) = \prod_{n=1}^N h_n^{j_n}(x_n), \quad (11)$$

and the tensor grid

$$\mathcal{X}_{\mathbf{j}} = \mathcal{X}_{1,j_1} \times \mathcal{X}_{2,j_2} \times \dots \times \mathcal{X}_{N,j_N}, \quad (12)$$

where each univariate grid $\mathcal{X}_{n,j_n} = \{x_{n,0}, x_{n,1}, \dots, x_{n,j_n}\}$ is assumed to be a Leja sequence. A multivariate hierarchical interpolation scheme can then be derived as follows. We consider a downward closed multi-index set Λ , such that

$$\forall \mathbf{j} \in \Lambda \Rightarrow \mathbf{j} - \mathbf{e}_n \in \Lambda, \forall n = 1, \dots, N, \quad (13)$$

where \mathbf{e}_n denotes the unit vector in the n th dimension. The associated interpolation grid is given by

$$\mathcal{X}_{\Lambda} = \bigcup_{\mathbf{j} \in \Lambda} \mathcal{X}_{\mathbf{j}}. \quad (14)$$

Since each multi-index $\mathbf{j} \in \Lambda$ uniquely defines a multivariate Leja node $\mathbf{x}_{\mathbf{j}} \in \mathcal{X}_{\Lambda}$, it holds that $\#\Lambda = \#\mathcal{X}_{\Lambda}$, where the symbol $\#$ denotes the cardinality of a set. Then, a sequence of nested, downward closed multi-index sets $(\Lambda_w)_{w=1}^W$, $\#\Lambda = W$, can be defined, such that $\Lambda_w = \{\mathbf{j}_1, \mathbf{j}_2, \dots, \mathbf{j}_w\}$, $\Lambda_{w-1} \subset \Lambda_w$ ($\Lambda_0 = \emptyset$), $\#\Lambda_w = w$, and $\Lambda_w \setminus \Lambda_{w-1} = \{\mathbf{j}_w\}$. This also implies that $\Lambda_1 = \{\mathbf{j}_1 = \mathbf{0} = (0, 0, \dots, 0)\}$. A corresponding grid sequence $(\mathcal{X}_{\Lambda_w})_{w=1}^W$ is similarly defined, where $\mathcal{X}_{\Lambda_w} = \{\mathbf{x}_{\mathbf{j}_1}, \mathbf{x}_{\mathbf{j}_2}, \dots, \mathbf{x}_{\mathbf{j}_w}\}$, $\mathcal{X}_{\Lambda_{w-1}} \subset \mathcal{X}_{\Lambda_w}$ ($\mathcal{X}_{\Lambda_0} = \emptyset$), $\#\mathcal{X}_{\Lambda_w} = w$, and $\mathcal{X}_{\Lambda_w} \setminus \mathcal{X}_{\Lambda_{w-1}} = \{\mathbf{x}_{\mathbf{j}_w}\}$, i.e. a single Leja node is added to the next grid in sequence, as in the univariate case. Simplifying the notation to $\mathbf{x}_{\mathbf{j}_w} = \mathbf{x}_w$ and $H_{\mathbf{j}_w}(\mathbf{x}) = H_w(\mathbf{x})$, the multivariate hierarchical interpolation reads

$$\tilde{g}(\mathbf{x}) = \mathcal{I}_{\Lambda}[g](\mathbf{x}) = \sum_{\mathbf{j} \in \Lambda} s_{\mathbf{j}} H_{\mathbf{j}}(\mathbf{x}) = \sum_{w=1}^W s_w H_w(\mathbf{x}) = \sum_{w=1}^W (g(\mathbf{x}_w) - \mathcal{I}_{\Lambda_{w-1}}[g](\mathbf{x}_w)) H_w(\mathbf{x}), \quad (15)$$

where $s_1 = s_0 = g(\mathbf{x}_1) = g(\mathbf{x}_0)$, i.e. \mathcal{I}_{Λ_0} is a null operator, similar to the univariate case.

The multivariate hierarchical Leja interpolation (15) can be constructed adaptively by means of a greedy algorithm^{24,25}, which sequentially adds terms of high impact to the polynomial approximation, while neglecting non-influential terms. The greedy algorithm, also known as a dimension-adaptive algorithm⁵¹, consists of the following steps.

1. A readily available hierarchical interpolation $\mathcal{I}_{\Lambda}[g](\mathbf{x})$ in the form of (15) is assumed to exist. Otherwise, the algorithm is initialized with the zero multi-index, such that $\Lambda = \{\mathbf{0}\}$.
2. The set of admissible neighboring multi-indices is computed, which is defined as

$$\Lambda^{\text{adm}} = \{\mathbf{j} \notin \Lambda : \mathbf{j} - \mathbf{e}_n \in \Lambda, \forall n = 1, \dots, N, \text{ with } j_n > 0\}, \quad (16)$$

such that $\Lambda \cup \{\mathbf{j}\}$ is a downward closed multi-index set $\forall \mathbf{j} \in \Lambda^{\text{adm}}$.

3. The hierarchical surpluses $\{s_{\mathbf{j}} = g(\mathbf{x}_{\mathbf{j}}) - \mathcal{I}_{\Lambda}[g](\mathbf{x}_{\mathbf{j}})\}_{\mathbf{j} \in \Lambda^{\text{adm}}}$ are computed.

4. The multi-index $\mathbf{j}_* \in \Lambda^{\text{adm}}$ is selected, where $s_{\mathbf{j}_*} = \text{argmax}_{\mathbf{j} \in \Lambda^{\text{adm}}} |s_{\mathbf{j}}|$.
5. The interpolation is updated such that $\Lambda \leftarrow \Lambda \cup \{\mathbf{j}_*\}$ and $\mathcal{X}_\Lambda \leftarrow \mathcal{X}_\Lambda \cup \{\mathbf{x}_{\mathbf{j}_*}\}$.
6. The steps (2) - (5) are repeated until the desired approximation accuracy or the maximum allowed number of model evaluations is reached.

3.3 | Polynomial chaos expansion on Leja grids

Similar to the stochastic collocation method presented in section 3.2, the PCE method^{53,54} also produces a global polynomial approximation $\tilde{g}(\mathbf{x}) \approx g(\mathbf{x})$, however, instead of Lagrange or hierarchical polynomials, the polynomial basis consists of orthonormal polynomials with respect to the PDF that characterizes the input parameters. Again, in the following, we consider a scalar model output $g(\mathbf{x}) \in \mathbb{R}$ for simplicity. The method can be applied component-wise to address vector-valued model outputs.

Considering a single parameter dependence, i.e. a model $g(x)$, the aforementioned orthonormality condition reads

$$\mathbb{E} [\psi^p \psi^q] = \int_{\Xi} \psi^p(x) \psi^q(x) \pi_X(x) dx = \delta_{pq}, \quad (17)$$

where $\mathbb{E} [\cdot]$ denotes the expectation operator, ψ^p and ψ^q are polynomials with degrees p and q , respectively, $\pi_X(x)$ is the univariate PDF, and δ_{ij} is the Kronecker delta. Depending on the PDF $\pi_X(x)$, the orthonormal polynomials can be chosen according to the Wiener-Askey scheme⁵⁴ or be constructed numerically^{43,55-58}. The univariate PCE is then given as

$$\tilde{g}(x) = \sum_{p=0}^P c_p \psi^p(x), \quad (18)$$

where c_p are scalar coefficients and P denotes the maximum polynomial degree.

In the multivariate case, recalling the assumption that the input RVs are independent (see section 2), multivariate orthonormal polynomials with respect to the PDF $\pi_{\mathbf{X}}(\mathbf{x}) = \prod_{n=1}^N \pi_{X_n}(x_n)$ can be constructed as products of univariate ones, such that

$$\Psi_{\mathbf{p}}(\mathbf{x}) = \prod_{n=1}^N \psi_n^{p_n}(x_n), \quad (19)$$

where $\mathbf{p} = (p_1, \dots, p_N)$ is a multi-index that comprises the univariate polynomial degrees. The corresponding orthonormality condition reads

$$\mathbb{E} [\Psi_{\mathbf{p}} \Psi_{\mathbf{q}}] = \int_{\Xi} \Psi_{\mathbf{p}}(\mathbf{x}) \Psi_{\mathbf{q}}(\mathbf{x}) \pi_{\mathbf{X}}(\mathbf{x}) dx = \delta_{\mathbf{pq}}, \quad (20)$$

where $\delta_{\mathbf{pq}} = \prod_{n=1}^N \delta_{p_n q_n}$ and the multivariate PCE is given by

$$\tilde{g}(\mathbf{x}) = \sum_{\mathbf{p} \in \Lambda} c_{\mathbf{p}} \Psi_{\mathbf{p}}(\mathbf{x}), \quad (21)$$

where Λ denotes a multi-index set that comprises the multi-indices of the multivariate PCE basis. Contrary to the multivariate hierarchical interpolation (15), the multi-index set Λ is not necessarily downward closed. There are numerous options for constructing the PCE basis, equivalently, for selecting the multi-index set Λ . One popular option is to use a so-called total degree (TD) basis, where

$$\Lambda_{\text{TD}} = \left\{ \mathbf{p} : \sum_{n=1}^N p_n \leq P, P \in \mathbb{Z}_{\geq 0} \right\}. \quad (22)$$

The downside of this choice is the isotropic handling of the input parameters leading to a basis size of $\frac{(N+P)!}{N!P!}$, whereas in most cases of practical interest certain parameters or parameter contributions have a stronger influence on the model output than others. Therefore, it is typically beneficial to construct so-called sparse PCEs⁵⁹⁻⁶³ by neglecting non-influential basis terms. Adaptive basis expansion algorithms are often used for that purpose⁶⁴⁻⁶⁹.

An alternative approach is to first compute an approximation by means of an interpolation based stochastic collocation method, e.g. using the dimension-adaptive algorithm presented in section 3.2 to omit non-influential terms, and then perform a transformation to an orthonormal polynomial basis⁷⁰⁻⁷². For the case of a hierarchical Leja interpolation $\mathcal{I}_{\Lambda}[g](\mathbf{x})$ given as in (15), this transformation proceeds as follows. First, the corresponding PCE basis $\{\Psi_{\mathbf{p}}\}_{\mathbf{p} \in \Lambda}$ is constructed using the same multi-index set Λ , thus establishing a one-to-one map between the hierarchical and the orthonormal basis polynomials. Next, using a

sequence of nested, downward closed multi-index sets as in section 3.2, i.e. $\Lambda_1 \subset \Lambda_2 \subset \dots \subset \Lambda$ with $\Lambda_w = \{\mathbf{p}_1, \mathbf{p}_2, \dots, \mathbf{p}_w\}$, $w = 1, \dots, W = \#\Lambda$, and employing the simplified notation $\mathbf{x}_{\mathbf{p}_w} = \mathbf{x}_w$ and $\Psi_{\mathbf{p}_w} = \Psi_w$, the design matrix $\mathbf{A} \in \mathbb{R}^{W \times W}$ with entries $a_{vw} = \Psi_w(\mathbf{x}_v)$ is computed. Last, the model evaluations on the Leja grid nodes are collected in a vector $\mathbf{g} = (g(\mathbf{x}_{\mathbf{p}}))_{\mathbf{p} \in \Lambda}$ and the PCE coefficients $\mathbf{c} = (c_{\mathbf{p}})_{\mathbf{p} \in \Lambda}$ are obtained by solving the linear system

$$\mathbf{A} \mathbf{c} = \mathbf{g}. \quad (23)$$

The linear system (23) is very simple to solve and its computational cost can be regarded as negligible next to other operations, e.g. compared to computationally demanding model evaluations $g(\mathbf{x}_w)$, $w = 1, \dots, W$. Nevertheless, efficient basis transformation methods⁷¹ can be employed in cases where the cost of the linear system solution must be taken into consideration.

An important aspect of the PCE is that it provides UQ metrics regarding the approximated model output, which are obtained with negligible computational cost by simply post-processing the PCE's terms. In particular, exploiting the orthonormality property of the basis polynomials, the mean value and the variance of the output can be estimated as

$$\mu = c_{\mathbf{0}} = c_1, \quad (24)$$

$$\sigma^2 = \sum_{\mathbf{p} \in \Lambda \setminus \{\mathbf{0}\}} c_{\mathbf{p}}^2 = \sum_{w=2}^W c_w^2. \quad (25)$$

Note that each PCE coefficient $c_{\mathbf{p}}$, $\mathbf{p} \in \Lambda \setminus \{\mathbf{0}\}$, corresponds to a partial variance that contributes to the total variance of the model output. Based on the known connection between variance based sensitivity analysis metrics^{73–75} and the PCE method^{31,76}, all PCE coefficients except for $c_{\mathbf{0}}$ can be interpreted as sensitivity indicators.

4 | MULTI-ELEMENT STOCHASTIC COLLOCATION WITH ADAPTIVE REFINEMENT

Global polynomial approximations face major difficulties in terms of accuracy and convergence when applied to problems with discontinuities in the parameter space. Additionally, steep gradients or large variations in the objective function also hinder the convergence of global approximation approaches. To address this bottleneck, several *multi-element* approximation techniques have been proposed^{10,13–16,18,77}, where the parameter space is decomposed into subspaces of improved regularity. Local polynomial approximations are developed in the subspaces, which are subsequently combined to provide a global surrogate model. Borrowing terminology from the finite element method (FEM) literature^{78–82}, we call *h*-refinement the refinement of the parameter domain decomposition with additional subdomains and *p*-refinement the refinement of a local polynomial approximation with additional terms. In the following, we build upon the Leja based hierarchical interpolation and PCE methods presented in Section 3 and develop a multi-element polynomial approximation method which refines adaptively both the parameter domain decomposition and the polynomial approximations according to the particularities of the problem at hand. Note that we use the notation \tilde{g}^{HI} and \tilde{g}^{PCE} to distinguish between surrogate models based on hierarchical interpolation and PCE, respectively.

4.1 | Multi-element hierarchical interpolation and polynomial chaos expansion

Let the image space of the random vector $\mathbf{X} = (X_1, \dots, X_N)$ be given as $\Xi = [a_1, b_1] \times [a_2, b_2] \times \dots \times [a_N, b_N]$, where $a_n, b_n \in \mathbb{R}$, $n = 1, \dots, N$, with extension to infinity. The image space is decomposed into K non-overlapping hypercubes, subsequently referred to as *elements*, such that $\Xi = \bigcup_{k=1}^K d_k$, where each element d_k is defined as $d_k = d_1^{(k)} \times d_2^{(k)} \times \dots \times d_N^{(k)}$ with $d_n^{(k)} = [a_n^{(k)}, b_n^{(k)}]$ if $n < N$ and $d_N^{(k)} = [a_N^{(k)}, b_N^{(k)}]$.

We proceed by introducing conditional expectations and local densities associated to the partition $\{d_k\}$. To that end, let $\mathbb{1}_k(\mathbf{x})$ denote the indicator function defined as

$$\mathbb{1}_k(\mathbf{x}) = \begin{cases} 1, & \mathbf{x} \in d_k, \\ 0, & \text{else.} \end{cases} \quad (26)$$

We write $Y_k = \mathbb{1}_k(\mathbf{X})$ in the following. Then,

$$\mathbb{E}[\mathbf{X}|Y_k = 1] = \frac{\mathbb{E}[\mathbf{X}Y_k]}{P(Y_k = 1)}, \quad k = 1, \dots, K. \quad (27)$$

We then use the definition of a PDF via an expected value

$$\pi_X(x) = \mathbb{E}[\delta(X - x)], \quad (28)$$

where δ denotes the Dirac delta distribution, to obtain conditional PDFs for the partition. In particular, we obtain

$$\pi_{\mathbf{X}}(\mathbf{x}|Y_k = 1) = \frac{\mathbb{E}[\delta(\mathbf{X} - \mathbf{x})Y_k]}{P(Y_k = 1)}, \quad (29)$$

$$\pi_k(\mathbf{x}^{(k)}) = \pi_{\mathbf{X}}(\mathbf{x}^{(k)}|Y_k = 1) = \frac{\pi_{\mathbf{X}}(\mathbf{x}^{(k)})}{\varrho_k}, \quad \text{for } \mathbf{x} = \mathbf{x}^{(k)} \in d_k. \quad (30)$$

The normalization factor $\varrho_k = \Pr(Y_k = 1)$ is determined as

$$\varrho_k = \prod_{n=1}^N \int_{a_n^{(k)}}^{b_n^{(k)}} \pi_{X_n}(x_n) dx_n. \quad (31)$$

In each element, a local interpolation grid $\mathcal{X}_{\Lambda^{(k)}}^{(k)}$ is generated following a local multi-index set $\Lambda^{(k)}$. In this work we consider multi-index sets either corresponding to a TD polynomial basis (see Section 3.3) or generated with the greedy-adaptive algorithm described in Section 3.2. The weighted Leja points in each element are obtained using the local PDFs, where the local univariate Leja sequences are defined as

$$x_{n,j_n}^{(k)} = \operatorname{argmax}_{x \in d_n^{(k)}} \sqrt{\pi_{X_n}(x) / \varrho_k} \prod_{i=0}^{j_n-1} |x - x_{n,i}^{(k)}|, \quad (32)$$

and correspond to local univariate interpolation grids $\mathcal{X}_{n,j_n}^{(k)} = \{x_{n,0}^{(k)}, x_{n,1}^{(k)}, \dots, x_{n,j_n}^{(k)}\} \subset d_n^{(k)}$. Local hierarchical polynomial interpolations $\tilde{g}_k^{\text{HI}}(\mathbf{x}) = \mathcal{I}_{\Lambda^{(k)}}[g](\mathbf{x})$, $\mathbf{x} \in d_k$, $k = 1, \dots, K$, can then be computed as described in Section 3.2 and subsequently be transformed into local PCEs $\tilde{g}_k^{\text{PCE}}(\mathbf{x})$ as shown in Section 3.3.

Once available, the local surrogate models are combined to form global surrogate models as

$$\tilde{g}^{\text{HI}}(\mathbf{x}) = \sum_{k=1}^K \mathbb{1}_k(\mathbf{x}) \tilde{g}_k^{\text{HI}}(\mathbf{x}), \quad (33a)$$

$$\tilde{g}^{\text{PCE}}(\mathbf{x}) = \sum_{k=1}^K \mathbb{1}_k(\mathbf{x}) \tilde{g}_k^{\text{PCE}}(\mathbf{x}). \quad (33b)$$

Using the PCE based global surrogate model, the mean and variance of the output can be estimated as

$$\mu = \sum_{k=1}^K c_{\mathbf{0}}^{(k)} \varrho_k, \quad (34)$$

$$\sigma^2 = \sum_{k=1}^K \left(\sigma_k^2 + (c_{\mathbf{0}}^{(k)} - \mu)^2 \right) \varrho_k, \quad (35)$$

where the local variances σ_k^2 are estimated as in (25)¹³. For uniformly distributed parameters, the local RVs $\mathbf{X}^{(k)}$ also follow a uniform distribution which can be easily normalized to the domain d_k , i.e. no additional costs for computing the normalization factors in (31) arise. This also allows the further use of Legendre polynomials for the PCE basis¹³. If non-uniform distributions are employed, the local orthonormal polynomials must be constructed numerically⁷⁷.

4.2 | *hp*-Adaptivity

Adaptive approximation strategies based on *hp*-refinement are widely used for FEM based approximations^{78–82}. Typically, these strategies follow the step sequence

$$\text{SOLVE} \Rightarrow \text{ESTIMATE} \Rightarrow \text{MARK} \Rightarrow \text{REFINE},$$

which is iterated until the desired approximation accuracy has been reached. The flowchart shown in Figure 1 provides a systematic overview of the *hp*-refinement procedure followed in this work for developing polynomial approximations by means of the suggested multi-element stochastic collocation method. The individual steps are explained in detail next.

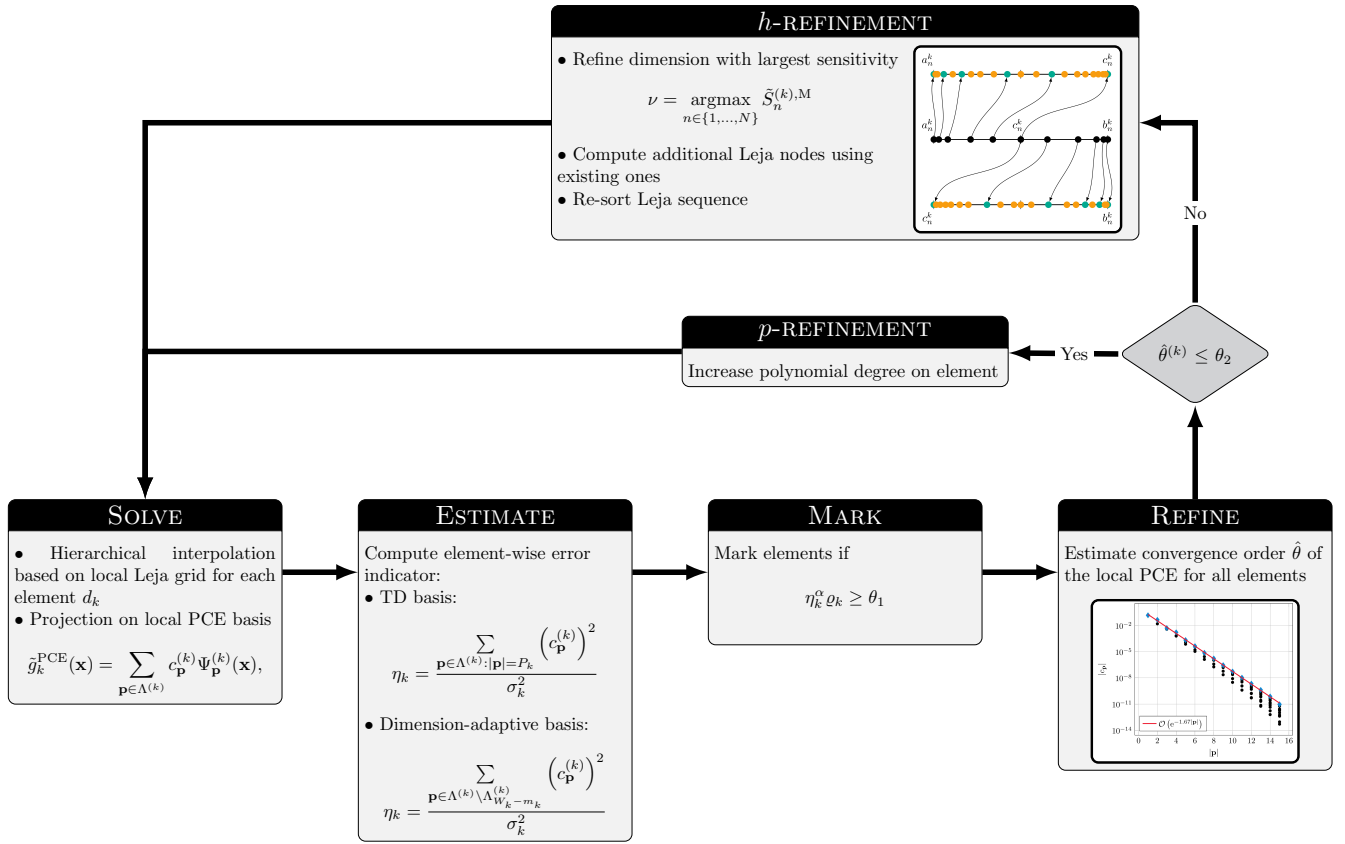


FIGURE 1 Sketch of the *hp*-adaptive multi-element stochastic collocation method.

4.2.1 | SOLVE

Given a decomposition of the parameter (image) space $\Xi = \bigcup_{k=1}^K d_k$, a hierarchical interpolation based on the local Leja grid $\mathcal{X}_{\Lambda^{(k)}}^{(k)}$ is computed in each element d_k . Subsequently, the local hierarchical polynomial bases are transformed to orthonormal ones, thus obtaining a local PCE in each element.

4.2.2 | ESTIMATE

To estimate the approximation quality of the local surrogate models in each element, local error indicators are employed¹³. Assuming an isotropic polynomial basis, e.g. the TD basis defined in (22), the error indicator is given by

$$\eta_k = \frac{\sum_{\mathbf{p} \in \Lambda^{(k)}: |\mathbf{p}|=P_k} (c_{\mathbf{p}}^{(k)})^2}{\sigma_k^2}, \quad (36)$$

where $P_k = \max_{\mathbf{p} \in \Lambda^{(k)}} |\mathbf{p}|$. The error indicator (36) relates the highest-order partial variances to the total variance in an element d_k . Thus, if the estimation on the local variance σ_k^2 is sufficiently accurate, the coefficients in the nominator of (36) will be small, thus resulting in a small error indicator value as well.

In the case of an anisotropic basis, e.g. obtained with the dimension-adaptive algorithm described in Section 3.2, the local multi-index set $\Lambda^{(k)}$ is of arbitrary shape, other than being downward closed. Then, the error indicator (36) might not be informative regarding the accuracy of the local polynomial approximation, e.g. considering multi-index sets with a single dominant dimension. To circumvent this problem, we propose a modified version of the error indicator (36), for which we search for the maximum polynomial degree P_k of a TD multi-index set, such that

$$\#\Lambda^{(k)} \geq \#\Lambda_{\text{TD}}^{(k)} = \binom{N + P_k}{N}. \quad (37)$$

The modified error indicator uses the m_k most recently added multi-indices in the set $\Lambda^{(k)}$, where the value of m_k is computed as

$$m_k = \binom{N + P_k}{N} - \binom{N + P_k - 1}{N}. \quad (38)$$

Assuming that $\#\Lambda^{(k)} = W_k$ and defining a nested sequence $\left\{ \Lambda_{w_k}^{(k)} \right\}_{w_k=1}^{W_k}$ where $\Lambda_{w_k}^{(k)}$ is downward closed and $\#\Lambda_{w_k}^{(k)} = w_k$, the last m_k multi-indices are included in the set $\Lambda^{(k)} \setminus \Lambda_{W_k - m_k}^{(k)}$. Then, the modified error indicator is given by

$$\eta_k = \frac{\sum_{\mathbf{p} \in \Lambda^{(k)} \setminus \Lambda_{W_k - m_k}^{(k)}} (c_{\mathbf{p}}^{(k)})^2}{\sigma_k^2}. \quad (39)$$

By employing m_k local PCE coefficients, the nominator in (39) contains the same number of partial variances as the nominator in (36) for a TD basis with total degree P_k . Due to the fact that the most recently added partial variances are employed, a similar behavior to the error indicator (36) is to be expected. Considering the widely arbitrary shape of the basis, the employed coefficients may origin from different polynomial levels, unlike in (36). It could therefore be beneficial to employ only the admissible coefficients of the dimension-adaptive algorithm, see section 3.2. However, for the considered examples, numerical tests showed that the proposed choice of coefficients is to be preferred.

4.2.3 | MARK

Given the local error indicators η_k , $k = 1, \dots, K$, an element d_k is marked for either h - or p -refinement if

$$\eta_k^\alpha \theta_k \geq \theta_1, \quad 0 < \alpha < 1, \quad (40)$$

where θ_1 , also referred to as the marking parameter, and α are user-defined constants. Regarding the choice of the values of these constants, an extensive discussion can be found in the literature¹³. For all numerical experiments presented in this work, the constant value $\alpha = 0.5$ is used, while θ_1 is varied according to the problem under investigation. Note that marking strategies other than the criterion stated in (40) can be adopted as well, e.g. the *fixed energy fraction* or the *maximum strategy* criteria suggested in the literature on hp -adaptive FEM^{78,80}. In contrast to criterion (40), these strategies mark elements if the local error indicator η_k is large compared to the error indicators of all remaining elements. However, our numerical experiments showed that the proposed marking strategy delivers slightly better results.

4.2.4 | REFINEMENT

Once the marking procedure is complete, a decision for either h - or p -refinement for each element d_k is made. To that end, the convergence order of the local PCE is estimated.

In deterministic FE-analysis, p -refinement is carried out if the solution is locally analytic on the element. In fact, the smoothness properties can be estimated from a Legendre expansion of the solution⁸³. In 1D, a linear model is fitted to the logarithmic values of the Legendre series and the slope \hat{m} is extracted. Then, p -refinement is carried out if $\hat{\theta} = e^{-\hat{m}}$ is above a certain threshold, corresponding to a sufficiently large Bernstein ellipse, hence, region of analyticity.

A similar approach can be applied to a (local) PCE approximation

$$\tilde{g}^{(k)}(\mathbf{x}) = \sum_{\mathbf{p} \in \Lambda^{(k)}} c_{\mathbf{p}}^{(k)} \Psi_{\mathbf{p}}^{(k)}(\mathbf{x}).$$

It has been shown⁸⁴ that for analytic functions the PCE coefficients satisfy

$$|c_{\mathbf{p}}^{(k)}| \leq C e^{-\sum_{n=1}^N a_n p_n}. \quad (41)$$

In fact, the result was proven for the Legendre basis, but it extends to other distributions with bounded support and regular density. The factors a_n describe the regularity in each dimension. In elements where the objective function $g(\mathbf{x})$ is smooth, a fast convergence, i.e. a large constant $a = \min_n a_n$ is expected, see e.g. Figure 2a. Contrarily, in elements where the objective function has less regularity, a small constant a is expected, as depicted in Figure 2b. Hence, an estimation on the convergence rate of the PCE coefficients can serve as an indicator for p , respectively h refinement. Hence, we define

$$\hat{\theta} = e^{-a}, \quad (42)$$

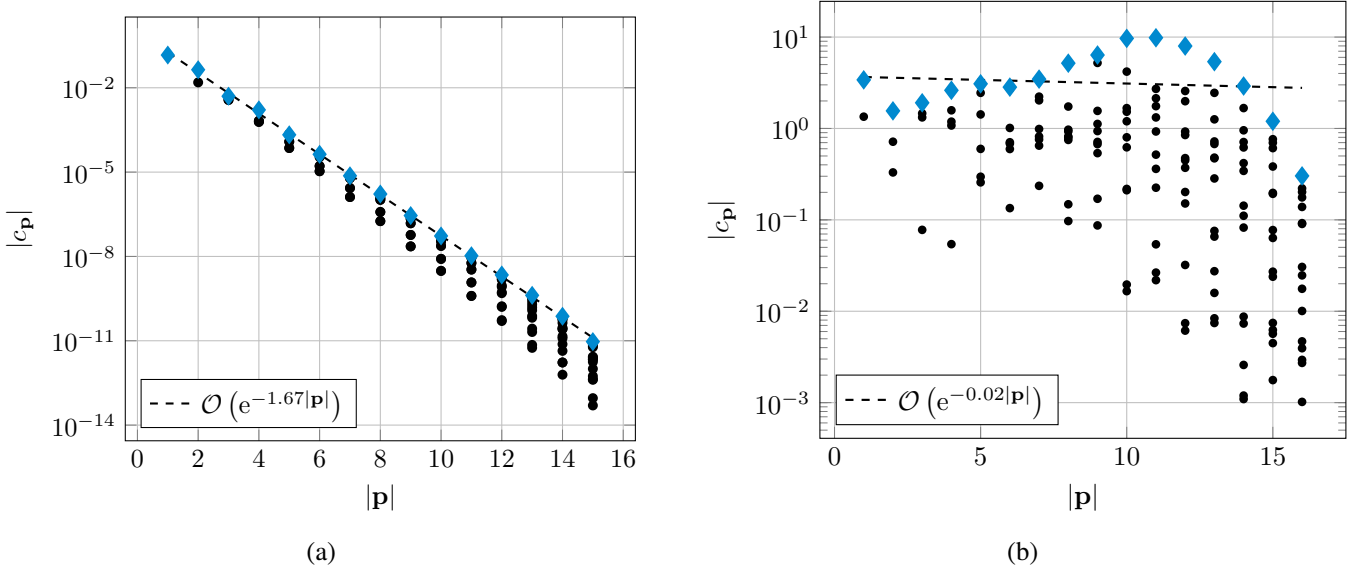


FIGURE 2 Estimating the decay of the PCE coefficients, (a) for a smooth objective function (b), for a function with reduced regularity. The blue markers show the coefficients employed to identify the rate of convergence.

as the convergence indicator. To estimate $\hat{\theta}$, a linear model with slope \hat{m} is fitted to the decaying PCE coefficients. The convergence indicator $\hat{\theta}$ is then estimated by solving

$$\begin{pmatrix} 1 & -1 \\ 1 & -2 \\ \vdots & \vdots \\ 1 & -P_k \end{pmatrix} \begin{pmatrix} b \\ \hat{m} \end{pmatrix} = \begin{pmatrix} \log(\max_{\mathbf{p} \in \Lambda^{(k)}: |\mathbf{p}|=1} |c_{\mathbf{p}}|) \\ \log(\max_{\mathbf{p} \in \Lambda^{(k)}: |\mathbf{p}|=2} |c_{\mathbf{p}}|) \\ \vdots \\ \log(\max_{\mathbf{p} \in \Lambda^{(k)}: |\mathbf{p}|=P_k} |c_{\mathbf{p}}|) \end{pmatrix} \quad (43)$$

in the least-squares sense and determined with $\hat{\theta} = e^{-\hat{m}}$. The decision for p - or h -refinement is then made with

$$\begin{aligned} p\text{-refinement}, \hat{\theta} &\leq \theta_2, \\ h\text{-refinement}, \hat{\theta} &> \theta_2, \end{aligned} \quad (44)$$

where θ_2 is a user-defined parameter.

***p*-Refinement**

In the case of p -refinement, the existing polynomial basis in an element d_k is extended with additional terms. If a TD basis is employed, the total degree P_k is increased by one and the Leja nodes corresponding to the newly added multi-indices are added to the interpolation grid. If an anisotropic basis is used, $\binom{N+P_k}{N} - \binom{N+P_k-1}{N}$ additional Leja points are included in the interpolation grid and the corresponding polynomial terms are added to the local surrogate model based on the greedy algorithm described in Section 3.2. In both cases, the already existing Leja grid points along with the corresponding function evaluations are reused, i.e. the original model must be evaluated only for the newly added Leja nodes.

***h*-Refinement**

In the case of h -refinement, for each parameter $X_n^{(k)}$, $n = 1, \dots, N$, in the element d_k , we estimate the main-effect Sobol sensitivity index^{73–75} using the local PCE, such that

$$\tilde{S}_n^{(k),M} = \frac{1}{\sigma_k^2} \sum_{\mathbf{p} \in \Lambda_n^{(k),M}} \left(c_{\mathbf{p}}^{(k)} \right)^2, \quad n = 1, \dots, N, \quad (45)$$

where

$$\Lambda_n^{(k),M} = \left\{ \mathbf{p} \in \Lambda^{(k)} : p_n \neq 0 \text{ and } p_m = 0, m \neq n \right\}. \quad (46)$$

The parameter that corresponds to the largest sensitivity index is then selected, i.e. the parameter X_v with

$$v = \operatorname{argmax}_{n \in \{1, \dots, N\}} \tilde{S}_n^{(k), M}, \quad (47)$$

and the corresponding univariate element $d_v^{(k)} = [a_v^{(k)}, b_v^{(k)}]$ is split into a “left” and a “right” element, $d_v^{(k), L} = [a_v^{(k)}, c_v^{(k)}]$ and $d_v^{(k), R} = [c_v^{(k)}, b_v^{(k)}]$, respectively, where the value of $c_v^{(k)}$ is chosen such that the two new elements have an equal probability mass, i.e.

$$\int_{a_v^{(k)}}^{c_v^{(k)}} \pi_{X_v}(x_v^{(k)}) \varrho_k dx_v^{(k)} = \frac{1}{2}. \quad (48)$$

Note that if $v = N$, then $d_v^{(k)} = [a_v^{(k)}, b_v^{(k)}]$. Accordingly, the univariate interpolation grid $\mathcal{X}_{v, j_v}^{(k)} = \{x_{v, 0}^{(k)}, x_{v, 1}^{(k)}, \dots, x_{v, j_v}^{(k)}\}$ that exists in the univariate element $d_v^{(k)}$ is split into a left grid $\mathcal{X}_{v, j_{v,L}}^{(k), L}$ and a right grid $\mathcal{X}_{v, j_{v,R}}^{(k), R}$, such that $\mathcal{X}_{v, j_v}^{(k)} = \mathcal{X}_{v, j_{v,L}}^{(k), L} \cup \mathcal{X}_{v, j_{v,R}}^{(k), R}$ and $\mathcal{X}_{v, j_{v,L}}^{(k), L} \cap \mathcal{X}_{v, j_{v,R}}^{(k), R} = \emptyset$. For $n \neq v$, the univariate elements $d_n^{(k)}$ and the corresponding univariate interpolation grids $\mathcal{X}_{n, j_n}^{(k)}$ remain unaffected. Therefore, the element d_k is also split into two new elements

$$d_k^L = d_1^{(k)} \times d_2^{(k)} \times \dots \times d_v^{(k), L} \times \dots \times d_N^{(k)}, \quad (49a)$$

$$d_k^R = d_1^{(k)} \times d_2^{(k)} \times \dots \times d_v^{(k), R} \times \dots \times d_N^{(k)}, \quad (49b)$$

with corresponding interpolation grids

$$\mathcal{X}_{\Lambda^{(k)}}^{(k), L} = \bigcup_{j \in \Lambda^{(k)}} \left(\mathcal{X}_{1, j_1}^{(k)} \times \mathcal{X}_{2, j_2}^{(k)} \times \dots \times \mathcal{X}_{v, j_{v,L}}^{(k), L} \times \dots \times \mathcal{X}_{N, j_N}^{(k)} \right), \quad (50a)$$

$$\mathcal{X}_{\Lambda^{(k)}}^{(k), R} = \bigcup_{j \in \Lambda^{(k)}} \left(\mathcal{X}_{1, j_1}^{(k)} \times \mathcal{X}_{2, j_2}^{(k)} \times \dots \times \mathcal{X}_{v, j_{v,R}}^{(k), R} \times \dots \times \mathcal{X}_{N, j_N}^{(k)} \right). \quad (50b)$$

We now shift our attention to $d_v^{(k)} = d_v^{(k), L} \cup d_v^{(k), R}$, since it is the only univariate element affected by the refinement of the element d_k . It can easily be observed that the interpolation grids $\mathcal{X}_{v, j_{v,L}}^{(k), L}$ and $\mathcal{X}_{v, j_{v,R}}^{(k), R}$ that result from splitting the original element, do not coincide with the Leja sequences that would be constructed in the elements $d_v^{(k), L}$ and $d_v^{(k), R}$, respectively, using the Leja sequence definition in (5) or (6). Therefore, the attractive properties of Leja sequences are mostly lost, especially their suitability as interpolation grids due to the subexponential growth of the Lebesgue constant⁴¹. Nevertheless, interpolation stability can be recovered by using the existing points to initialize a Leja sequence and then add new Leja points computed as in the definitions (5) and (6), a procedure called *stabilization*³⁵. Additionally, the stabilized interpolation grid is sorted according to the Leja ordering, which is necessary to achieve improved Lebesgue constant values^{35,38}.

The stabilization procedure and its relation to the Lebesgue constant is illustrated in Figure 3. We consider an initial domain $[-1, 1]$ with a corresponding Leja sequence consisting of eleven points, which is split into $[-1, 0)$ and $[0, 1]$, and focus on the latter subdomain. Figure 3a shows the initial Leja sequence (black nodes) and the six points that are re-used within subdomain $[0, 1]$ (green nodes). The re-used points are used to initialize a Leja sequence and compute new points (orange nodes) until the interpolation grid is stabilized. For comparison, the Leja points calculated in the interval $[0, 1]$ without prior initialization are shown (blue nodes), where it is obvious that they do not coincide with the points of the stabilized Leja grid. Figure 3b shows the Lebesgue constant for an increasing number of interpolation points for the stabilized grid in $[0, 1]$, where the initial six points (denoted with green) are obtained from the readily available Leja sequence within $[-1, 1]$ prior to splitting. For comparison, the Lebesgue constant for Chebyshev points and for Leja points without prior initialization within $[0, 1]$ are shown. It can easily be observed that adding new nodes according to the Leja sequence definition results in the reduction and stabilization of the Lebesgue constant. It is also clear that sorting the stabilized grid according to the Leja ordering is crucial for interpolation stability.

Remark: In the proposed approach, the new elements employ the same multi-index set as the original element. Subsequently, all function evaluations are preserved. In the presented numerical examples this will always be the case if a TD basis is employed. However, in cases where a dimension-adaptive basis is used, the new elements most likely feature an anisotropic behavior different than the original element. Therefore, the multi-index sets in the new elements are re-initialized with the multi-index set $\Lambda = \{\mathbf{0}\}$. The grid defined in (50) then acts as a depot, where Leja nodes are picked if the adaptive Leja algorithm demands for the corresponding nodes. The univariate grids are only extended if all already existing nodes have been utilized. As a result, the recycling of all Leja points and function evaluations is not guaranteed in the case of adaptively constructed bases.

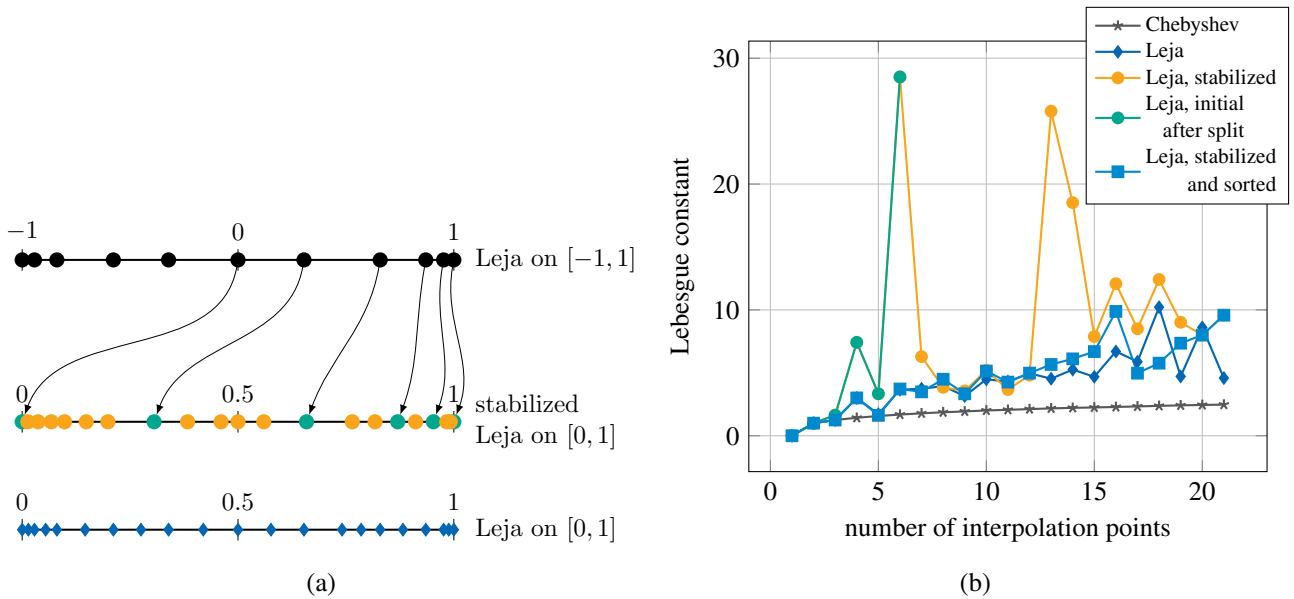


FIGURE 3 (a) Domain splitting and stabilization of the Leja points. The black points have been calculated for a uniform RV $X \sim \mathcal{U}[-1, 1]$. The green points show the readily available interpolation nodes within $[0, 1]$ after splitting the initial image space $[-1, 1]$, whereas the orange points are the new points which are calculated for the uniform RV $X \sim \mathcal{U}[0, 1]$ by considering the available (green) points as initialization for the Leja sequence. For comparison, the Leja sequence calculated for $X \sim \mathcal{U}[0, 1]$ without considering the readily available nodes are shown in blue. (b) Lebesgue constant for different interpolation grids.

5 | NUMERICAL EXPERIMENTS

In the following, the performance and approximation capabilities of the proposed hp -adaptive stochastic collocation method is tested on several test cases. A rigorous discussion on the h -convergence of the multi-element collocation method, in particular with isotropic and equidistant grids, is available in the literature¹⁴. Since the main advantage of using Leja sequences is the ability to re-use readily available Leja points and thus significantly reduce the computational cost due to the model evaluations on the collocation points, we focus on the computational gains provided by the h -adaptive and hp -adaptive refinement strategies described in Section 4. In particular, we first consider fixed polynomial bases, thus disregarding p -adaptivity, and compare the h -adaptive multi-element stochastic approach developed in this work against other h -adaptive multi-element methods found in the literature^{13,14}. Next, the hp -adaptive multi-element stochastic collocation method is applied to a one-dimensional analytical function and to a Bayesian inverse problem featuring two and five dimensions, respectively. Unless stated otherwise, a discrete root mean square (RMS) error is used to evaluate the convergence behavior of the tested methods. The error is given by

$$\epsilon_{\text{RMS}} = \sqrt{\mathbb{E}_Q [(\tilde{g}(\mathbf{x}) - g(\mathbf{x}))^2]} = \sqrt{\frac{1}{Q} \sum_{q=1}^Q (\tilde{g}(\mathbf{x}_q) - g(\mathbf{x}_q))^2}, \quad (51)$$

which is computed using a validation sample $\{\mathbf{x}_q\}_{q=1}^Q$ drawn randomly from the joint input PDF.

5.1 | h -Refinement test cases

5.1.1 | Discontinuous Gentz function

In this test case, we discuss the cost savings that are obtained when re-using the Leja points in the context of h -refinement. To that end, we consider the discontinuous Gentz function,

$$g(\mathbf{x}) = \begin{cases} 0, & \text{if } x_1 > u_1 \text{ and } x_2 > u_2, \\ \exp(a_1 x_1 + a_2 x_2), & \text{otherwise,} \end{cases} \quad (52)$$

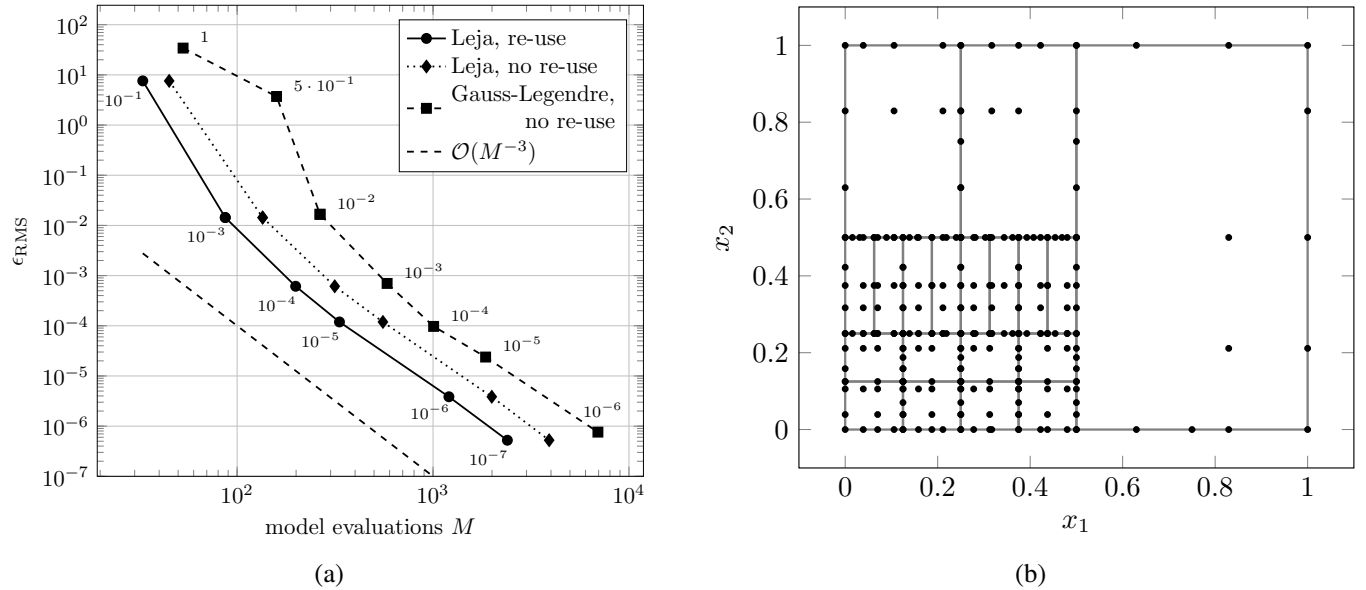


FIGURE 4 (a) RMS error versus model evaluations (M) for the multi-element stochastic collocation method based on Leja points with and without information re-use, as well as with Gauss-Legendre nodes. The marking parameter θ_1 is shown next to the marks, which show the results after the h -refinement procedure has converged. (b) Leja interpolation grid after the convergence of the h -refinement procedure for $\theta_1 = 10^{-3}$.

with $u_1 = u_2 = 0.5$, $a_1 = 5$, and $a_2 = 2.5$. In the following, x_1 and x_2 denote realizations of the RVs $X_1 \sim \mathcal{U}[0, 1]$ and $X_2 \sim \mathcal{U}[0, 1]$. The h -convergence is examined for varying values of the marking parameter θ_1 . Additionally, a comparison against the same methodology but based on Gauss-Legendre nodes is performed. In both cases, a TD polynomial basis with maximum polynomial degrees $P_k = 4$ in each element is used.

Figure 4a shows the RMS error (51) computed with a validation set of size $Q = 10^6$, in dependence to the number of function calls after the h -refinement procedure has converged for a given value of the marking parameter θ_1 . As can be observed, the Leja based stochastic collocation method outperforms the Gauss-Legendre based one, irrespective of whether the Leja nodes are re-used or not. By re-using the Leja nodes, an additional gain in performance is obtained. All employed approaches reach an asymptotic h -convergence rate of $\mathcal{O}(M^{-3})$ once the discontinuity of the function has been isolated. Figure 4b shows the interpolation grid and the corresponding Leja nodes after the h -adaptive algorithm has converged for $\theta_1 = 10^{-3}$. It is clearly visible that the adaptive h -refinement results in element splitting only in the regions of the parameter domain where the objective function is not zero, thus verifying that the h -refinement strategy and the corresponding refinement criteria described in Section 4.2.4 perform as expected.

5.1.2 | Kraichnan–Orszag three-mode problem

The Kraichnan–Orszag (KO) problem⁸⁵ is a three-term ordinary differential equation (ODE) that is often used in the literature to showcase the limitations of global polynomial models when applied to approximate dynamical models, which in this case is attributed to the reduced regularity arising from the stochastic initial conditions^{13,14,19,27}. The transformed KO problem reads

$$\begin{aligned} \frac{dy_1}{dt} &= y_1 y_3, \\ \frac{dy_2}{dt} &= -y_2 y_3, \\ \frac{dy_3}{dt} &= -y_1^2 + y_2^2, \end{aligned} \tag{53}$$

which is completed with the initial values

$$y_1(t=0) = y_1(0), \quad y_2(t=0) = y_2(0), \quad y_3(t=0) = y_3(0). \tag{54}$$

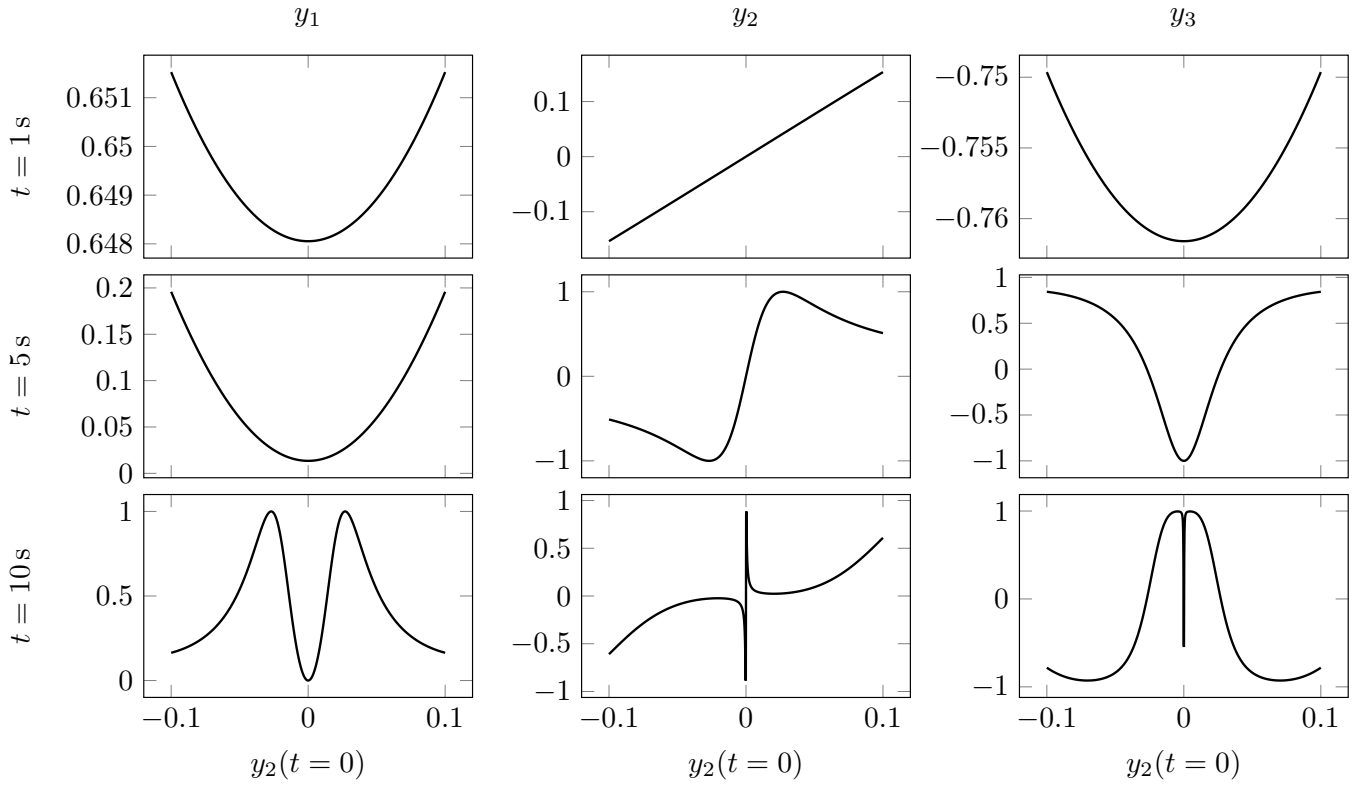


FIGURE 5 Solution to the Kraichnan–Orszag problem at different time steps in dependence of $y_2(t = 0)$. The results have been computed with $y_1(t = 0) = 1$, $y_3(t = 0) = 0$.

Figure 5 shows the solution to problem (53) for $y_1(t = 0) = 1$, $y_3(t = 0) = 0$ and a varying initial condition $y_2(t = 0)$. The plots illustrate clearly that the solution has a reduced regularity with respect to $y_2(t = 0)$, which is the reason why global polynomial approximations fail altogether.

In the following, the Leja based multi-element stochastic collocation method developed in this work is compared against a previously suggested multi-element method¹⁴. For all results presented next, a fourth-order Runge–Kutta integration scheme with a time stepping size of $\Delta t = 0.1$ s is employed to solve the KO problem (53). The accuracy of the surrogate models is evaluated based on the variance $\mathbb{V}[y_1(t)]$. That is, since a surrogate model for $y_1(y_2(t = 0))$ is constructed at each time step, the approximation accuracy is estimated using a normalized RMS error, defined as

$$\epsilon_{\text{RMS},t} = \sqrt{\frac{\sum_{i=1}^{N_t} (\mathbb{V}[\tilde{y}_1(t_i)] - \mathbb{V}[y(t_i)])^2}{\sum_{i=1}^{N_t} \mathbb{V}[y(t_i)]^2}}, \quad (55)$$

where N_t denotes the number of time steps. Furthermore, adaptive h -refinement is performed at each time step, such that the overall computational cost due to model evaluations amounts to

$$C = \sum_{i=1}^{N_t} M_{t_i}, \quad (56)$$

where M_{t_i} denotes the number of model evaluations to construct a surrogate model for time step t_i .

The 2D KO-problem is now determined with the random initial conditions

$$y_1(t = 0) = x_1, \quad y_2(t = 0) = 0.1x_2, \quad y_3(t = 0) = 0, \quad (57)$$

where x_1 and x_2 are realizations of uniformly distributed RVs in $[-1, 1]$ and $t \in [0, 10$ s]. The reference solution is calculated using a quasi Monte Carlo algorithm based on Sobol sequences and 10^7 samples. Figure 6 shows the time averaged RMS error of the variance $\mathbb{V}[y_1]$ over the number of total model evaluations C . Again, the h -convergence is analyzed for different values

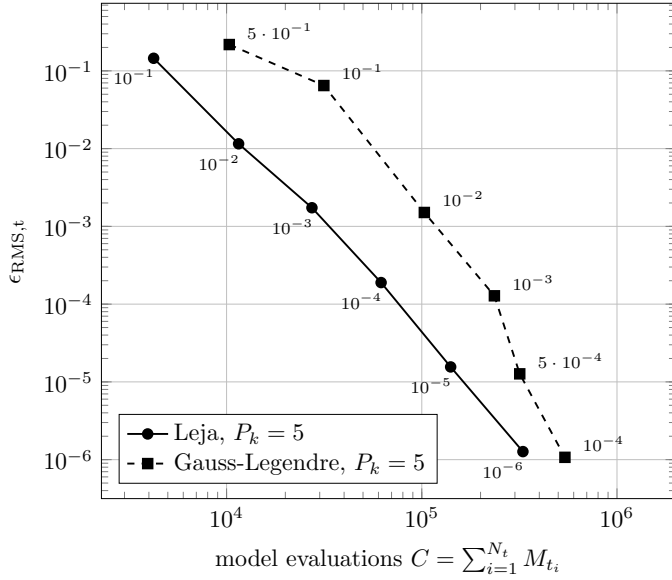


FIGURE 6 Time averaged RMS error of the variance $\mathbb{V}[y_1]$ versus the total number of model evaluations for the multi-element collocation method based on Leja nodes and Gauss-Legendre nodes, for different values of the marking parameter θ_1 . The results shown for a specific value of θ_1 refer to the converged h -refinement procedure.

of θ_1 , for Leja nodes and Gauss-Legendre nodes. A TD basis with maximum polynomial degree $P_k = 5$ is employed for all elements. The convergence plots clearly show that the use of Leja nodes results in significant performance gains, which is mainly attributed to re-using previously computed Leja nodes and the corresponding model evaluations.

5.2 | hp -Refinement test cases

5.2.1 | Analytical function

To showcase the computational benefits obtained due to the hp -adaptivity of the proposed method, an academic test case featuring a one-dimensional function is considered first. In particular, the analytical function

$$g(x) = -x + 0.1 \sin(30x) + e^{-(50(x-0.65))^2}, \quad (58)$$

is employed, which has previously been used to validate the Spectral Stochastic Embedding (SSE) method⁸⁶. The function is depicted in Figure 7a, where the values of the parameter x refer to realizations of the uniform RV $X \sim \mathcal{U}[0, 1]$. The observed sharp spike is the main reason why a rather slow convergence rate is to be expected if a global approximation is applied, e.g., a global interpolation on Leja or Chebychev nodes. The hp -adaptive Leja based multi-element collocation method should significantly improve the convergence rate by dividing the domain into smooth sub-domains (h -refinement), in which local polynomial approximations with increasing degree are developed (p -refinement), as presented in Section 4.

Following the SSE paper⁸⁶, the accuracy of a surrogate model $\tilde{g}(x) \approx g(x)$ is evaluated using the relative root mean squared error

$$\eta = \sqrt{\frac{\mathbb{E}[(g(x) - \tilde{g}(x))^2]}{\mathbb{V}[g(x)]}}, \quad (59)$$

which is estimated using a random sample with 10^5 points. The results for different surrogate models are shown in Figure 7b. The results for the hp -adaptive Leja based multi-element collocation method are obtained with $\theta_1 = 10^{-12}$ and $\theta_2 = 0.8$. Using h -refinement alone and a constant polynomial degree $P_k = 3$ leads to a convergence rate of $\mathcal{O}(M^{-4})$. For comparison, the results obtained with p -refined global interpolations on Leja and Chebyshev nodes, as well as with the SSE method⁸⁶ are presented.

All proposed methods show a converging behavior, however, it is clearly evident that the hp -adaptive multi-element collocation method outperforms all other surrogate modeling options. Based on a least-squares estimate on the decay of the error for the hp -adaptive approach, a geometric convergence rate⁸⁷ of $\mathcal{O}(e^{-0.32M})$ is obtained. Note that the hp -adaptive Leja based multi-element stochastic collocation method and the SSE method⁸⁶ tackle different types of problems. The method proposed in this

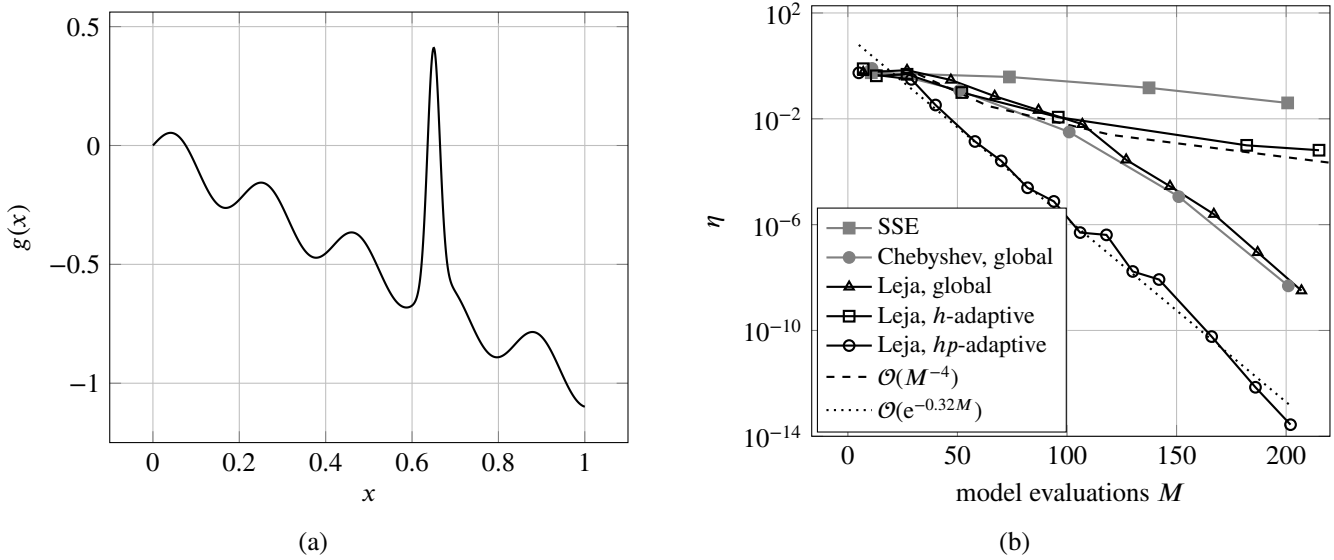


FIGURE 7 (a) One-dimensional analytical function. (b) Relative mean square error η in dependence of the number of model evaluations for SSE, global Chebyshev/Leja, and hp -adaptive Leja surrogates.

work handles problems with low to moderate dimensions, whereas the SSE method is intended for high dimensional problems. Therefore, the comparison in Figure 7b is not to be understood in a competing manner.

Next we analyze the impact of the parameters θ_1 and θ_2 on the hp -refinement procedure. Figure 8 shows the domain decomposition and the polynomial degree of each element for different values of θ_1 and θ_2 . The left column figures correspond to $\theta_1 = 10^{-2}$, while the right column figures to $\theta_1 = 10^{-4}$. Accordingly, the top row figures correspond to $\theta_2 = 0.2$, in which case h -refinement is preferred over p -refinement. Contrarily, p -refinement is prioritized in the bottom row figures, which correspond to $\theta_2 = 0.8$. An initial polynomial degree of $P_k = 2$ has been used for all four cases. All four choices for θ_1 and θ_2 generate interpolation grids that isolate the spike. As would be expected, more elements are generated for $\theta_2 = 0.2$, in particular in the region where the spike is observed. Further decreasing θ_1 leads to a more finely resolved spike area, where the polynomial degrees in each element remain at moderate values. As would also be expected, larger elements with higher polynomial degrees are generated for $\theta_2 = 0.8$. If θ_1 is further decreased in this case, p -refinement with a focus on the spike region is carried out.

5.2.2 | Posterior estimation

As stressed in section 1, surrogate models for the likelihood function, respectively for the posterior distribution of inverse problems, can be an alternative to expensive Markov chain Monte Carlo analysis. To showcase the benefits of using the method proposed in this work, a linear statistical model with additive noise is considered³, which reads

$$\mathbf{G}\mathbf{x} + \boldsymbol{\varepsilon} = \mathbf{b}, \quad (60)$$

where $\mathbf{b} \in \mathbb{R}^D$ denotes the observations or measurements, $\mathbf{x} \in \mathbb{R}^N$ the unknown model parameters, $\mathbf{G} \in \mathbb{R}^{D \times N}$ the forward model, and $\boldsymbol{\varepsilon} \in \mathbb{R}^D$ the Gaussian noise, such that $\boldsymbol{\varepsilon} \sim \mathcal{N}(0, \sigma^2 \mathbf{I})$, with $\mathbf{I} \in \mathbb{R}^{D \times D}$ being the identity matrix. Accordingly, it holds that $\mathcal{G}(\mathbf{x}) = \mathbf{G}\mathbf{x}$ for the likelihood function defined in (4). In the simplest case, the inverse problem (60) represents a linear regression problem, where \mathbf{G} is the discretized model operator and \mathbf{x} the vector of regression coefficients. In the same context, deconvolution problems pose significantly greater challenges.

The unknown parameter vector \mathbf{x} can be computed by means of maximum likelihood estimation (MLE), such that

$$\mathbf{x} = \underset{\mathbf{x}}{\operatorname{argmax}} L(\mathbf{x}|\mathbf{b}) = \underset{\mathbf{x}}{\operatorname{argmax}} \frac{1}{(2\pi)^{D/2}\sigma^D} \exp\left(-\frac{\|\mathbf{G}\mathbf{x} - \mathbf{b}\|^2}{2\sigma^2}\right), \quad (61)$$

where $L(\mathbf{x}|\mathbf{b})$ denotes the likelihood function. However, inverse problems are often ill-posed, e.g. due to the amplification of the measurement noise, thus resulting in very challenging parameter estimation tasks. A possible remedy is to regularize problem (60) by employing, e.g. Tikhonov regularization or iterative regularization^{3,88}, to name but a few options. Another measure is to

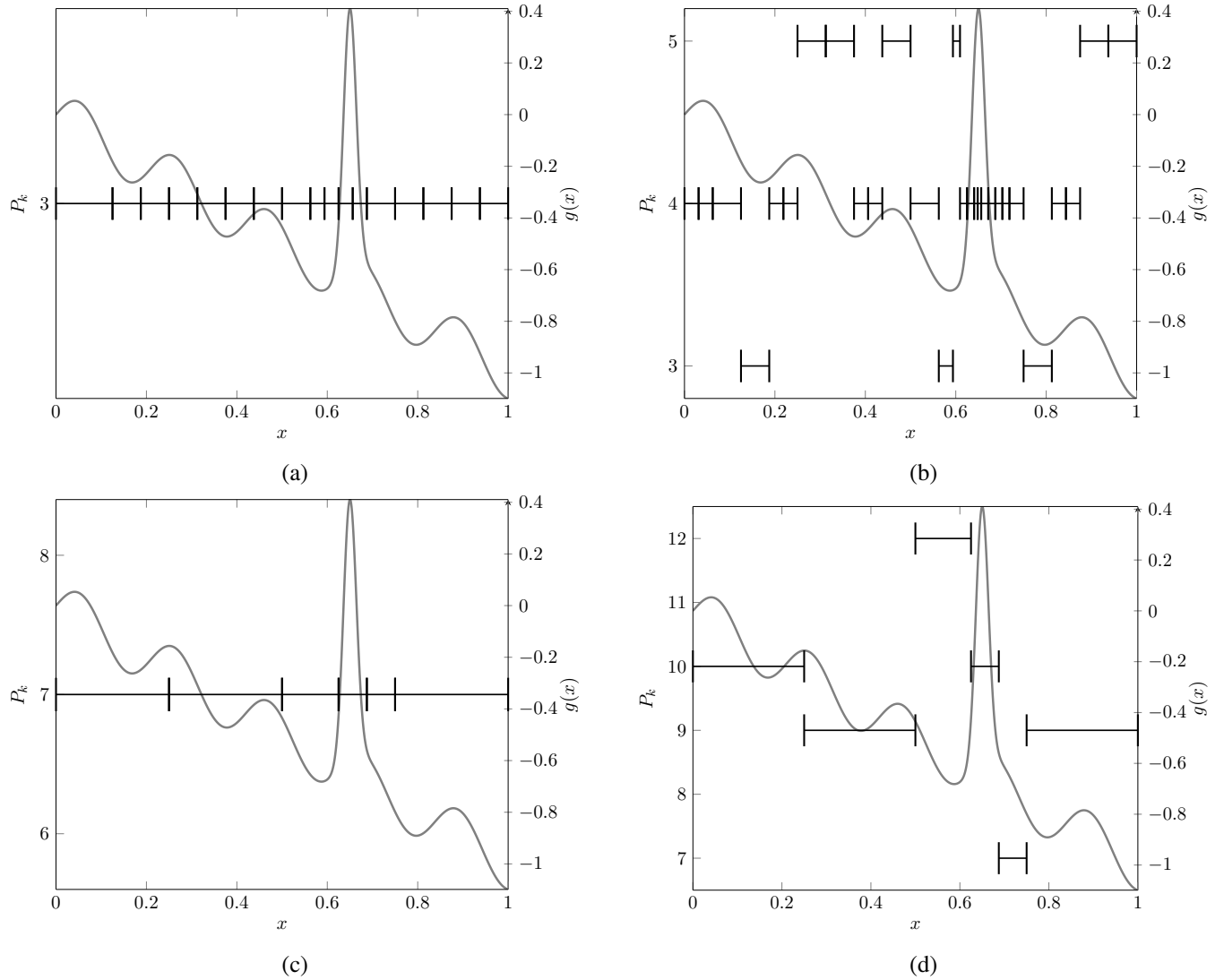


FIGURE 8 Adaptively generated interpolation grids and corresponding polynomial degrees for different values of θ_1 and θ_2 . (a) $\theta_1 = 10^{-2}, \theta_2 = 0.2$. (b) $\theta_1 = 10^{-4}, \theta_2 = 0.2$. (c) $\theta_1 = 10^{-2}, \theta_2 = 0.8$. (d) $\theta_1 = 10^{-4}, \theta_2 = 0.8$.

utilize Bayesian inference⁸⁸. Therein, the parameters \mathbf{x} are modelled as RVs and a prior distribution is assumed for them. Given the observations \mathbf{b} , information about the noise, and our prior belief regarding the parameter vector \mathbf{x} , Bayes' theorem yields

$$\pi(\mathbf{x}|\mathbf{b}) \propto L(\mathbf{x}|\mathbf{b})p(\mathbf{x}), \quad (62)$$

where $p(\mathbf{x})$ denotes the prior distribution and $\pi(\mathbf{x}|\mathbf{b})$ the posterior distribution. The posterior distribution (62) is now regularized by the prior distribution $p(\mathbf{x})$. The parameter vector can be estimated by maximizing (62), which leads to the so-called maximum a posteriori (MAP) estimation.

Using the Bayesian approach, additional statistical quantities that characterize the posterior distribution, e.g. its mean, variance, or higher-order moments, can be computed. In that case, the evidence, also referred to as the marginal likelihood, i.e. the normalization of (62) over the parameter vector \mathbf{x} , must be computed. The computation of the evidence can be challenging, as the likelihood function and thus also the posterior can be highly concentrated, see Figure 9a. The proposed multi-element collocation method can then be employed to obtain a surrogate model of (62), such that the evidence and the statistical moments can be computed accurately with a comparatively lower computational cost.

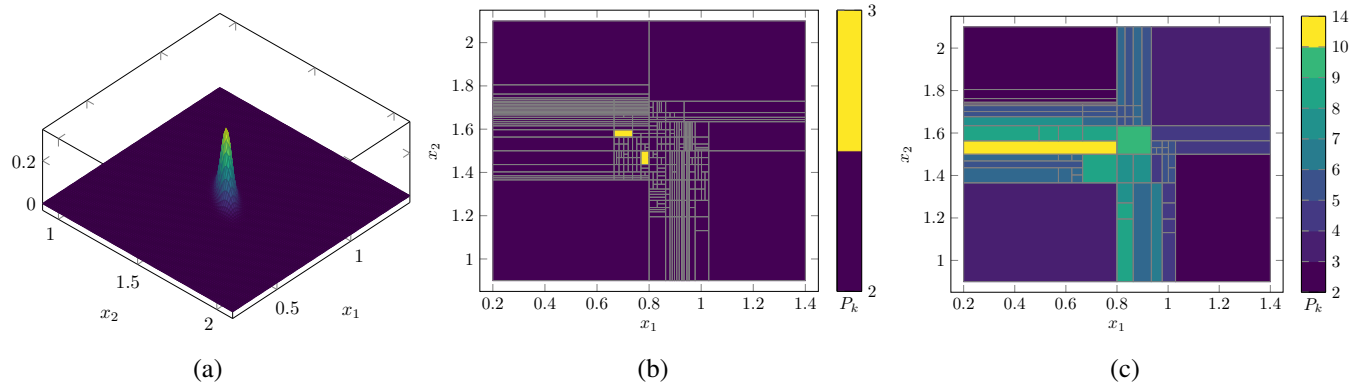


FIGURE 9 (a) Posterior over the parameters x_1 and x_2 . (b,c) Adaptively generated interpolation grids and corresponding polynomial degrees for $\theta_1 = 10^{-3}$ and different values of θ_2 . (b) $\theta_2 = 0.2$. (c) $\theta_2 = 0.8$.

Two-dimensional regression problem

We start with a two-dimensional linear regression test case where we search for the model parameters x_1 and x_2 such that the mapping $\xi \mapsto G(\xi, x_1, x_2)$ fits best to available measurement data. The model $G(\xi, x_1, x_2)$ reads

$$G(\xi, x_1, x_2) = x_2 \exp(x_1 \xi) - 2. \quad (63)$$

A measurement set with 5 noisy observations is assumed to be available, i.e. $\{\xi_i, b_i\}_{i=1}^5$, where ξ_i are equidistantly sampled in $[-1, 1]$. Artificial observations are then generated as $b_i = G(\xi_i, x_1^*, x_2^*) + \varepsilon$, where $\varepsilon \sim \mathcal{N}(0, \sigma^2)$ with $\sigma^2 = 0.01$. Note that x_1^* and x_2^* denote the true but currently unknown model parameters. We assume the parameters to follow a truncated normal distribution, denoted as $\mathcal{T}\mathcal{N}(\mu, \sigma^2, \ell, u)$, where μ and σ^2 are the mean and variance of a Gaussian distribution $\mathcal{N}(\mu, \sigma^2)$ which is truncated within the interval $[\ell, u]$. The parameter priors are given as $x_1 \sim \mathcal{T}\mathcal{N}(0.8, 0.04, 0.2, 1.4)$, $x_2 \sim \mathcal{T}\mathcal{N}(1.5, 0.04, 0.9, 2.1)$.

The posterior distribution is depicted in Figure 9a, which shows the strongly concentrated posterior density. Figure 10a shows the RMS error versus the number of model evaluations using stochastic collocation on Leja interpolation grids based on h -refinement, global interpolation with p -refinement, and hp -refinement with a varying adaptivity parameter θ_2 . All local polynomial approximations are based on TD bases. Except for p -refinement, all marks show the results after convergence for a specific marking parameter θ_1 . The results clearly show that surrogates based on h - and hp -refinement are superior to the global collocation approach. For a moderate number of model evaluations, a similar performance is observed using either h - or hp -refinement. However, once the parameter domain has been sufficiently decomposed, in which case the hp -adaptive algorithm prefers p - over h -refinement, hp -adaptivity yields significant computational gains. Additionally, at this point, a switch from an algebraic to a geometric convergence rate is observed.

Figures 9b and 9c show the domain decomposition as well as the employed polynomial degrees P_k of the local TD bases, for $\theta_2 = 0.2$ and $\theta_2 = 0.8$, respectively. The results correspond to the converged algorithm for a marking parameter $\theta_1 = 10^{-3}$. Both figures clearly illustrate that the hp -adaptive approach identifies the highly concentrated posterior density. As expected, in the case of $\theta_2 = 0.2$, more elements are spent to isolate the posterior density, while the local polynomial degrees P_k have low values. Contrarily, choosing $\theta_2 = 0.8$ results in fewer elements with significantly higher local polynomial degrees.

Four-dimensional deconvolution problem

We now consider a posterior estimation problem featuring four parameters. We again solve the inverse problem (60) for the parameter vector \mathbf{x} and given observations \mathbf{b} , however, the underlying problem is now a convolution problem of the form

$$b(t) = \int_{-\infty}^{\infty} g(t - t') x(t') dt', \quad -\infty \leq t \leq \infty, \quad (64)$$

where $b(t)$ is the output function, $g(t)$ is the weighting function or kernel, and $x(t)$ the input function. For example, in the field of acoustics, $b(t)$ is the system response, $g(t)$ the fundamental solution of the wave equation, and $x(t)$ the acting forces. The example can be found in the book of Bardsley³, where a detailed description of the functions and parameters is given. A MATLAB

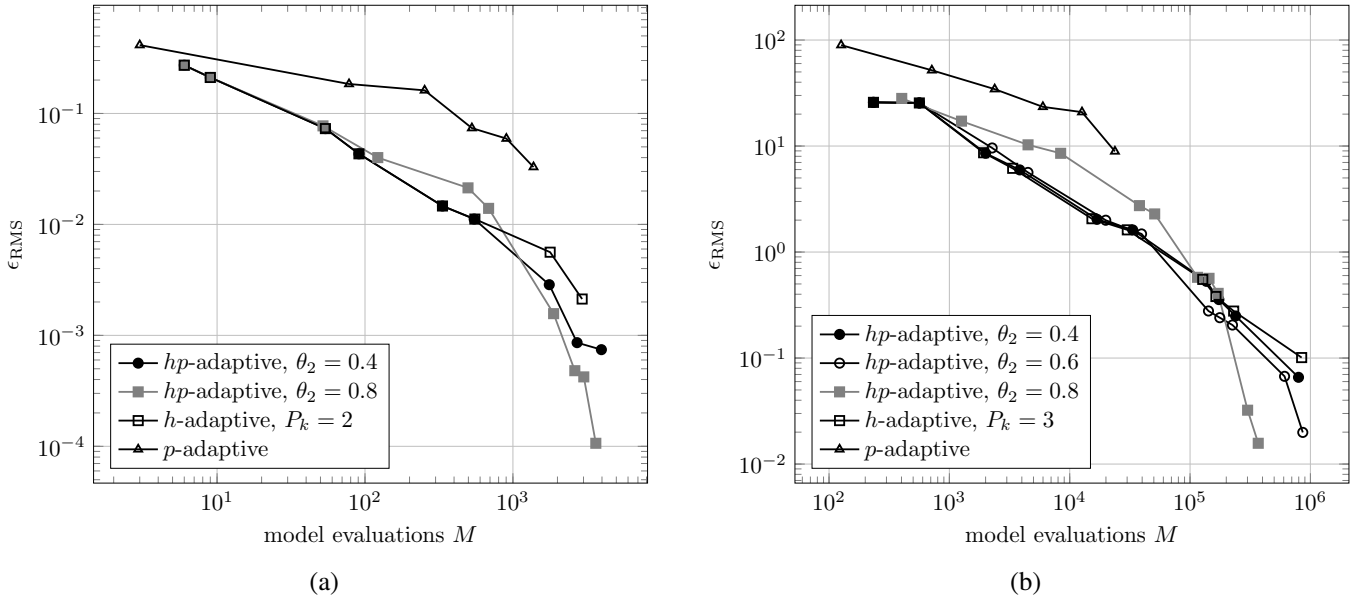


FIGURE 10 Convergence of the RMS error in dependence to model evaluations. The results have been obtained using TD polynomial bases. (a) Two-dimensional regression problem. (b) Four-dimensional deconvolution problem.

TABLE 1 Distribution of the random variables for the 4D Bayesian example.

parameter	distribution
x_1	$\mathcal{T}\mathcal{N}(0.88, 0.16, -0.32, 2.08)$
x_2	$\mathcal{T}\mathcal{N}(0.1, 0.04, -0.5, 0.7)$
x_3	$\mathcal{T}\mathcal{N}(0.3, 0.01, 0, 0.6)$
x_4	$\mathcal{T}\mathcal{N}(0.29, 0.01, -0.01, 0.59)$

implementation is also available⁸⁹. The convolution problem is discretized with 4 grid points, which leads to the discrete system (60). At each of the grid points, the unknown input values x_1, \dots, x_4 , are to be estimated based on the available data \mathbf{b} . Truncated normal distributions are considered as priors for the unknown input values, see Table 1. Furthermore, the measurements \mathbf{b} are polluted by additive Gaussian noise with $\sigma = 0.1$. The other parameters remain as in the book of Bardsley³.

Figure 10b shows the convergence of the RMS error over the number of model evaluations M . Similar to the two-dimensional case, all local polynomial approximations employ TD bases. As previously observed, once the concentrated posterior density has been sufficiently resolved by the algorithm, the collocation based on *hp*-refinement outperforms *h*-refinement alone. Moreover, it must be noted that, in this test case, the computational cost for constructing the Leja grid in the global *p*-refinement case, cannot be regarded to be negligible anymore due to the increasing costs of resolving the optimization problem (6). Therefore, the *hp*-adaptive stochastic collocation is to be preferred overall.

Remark: In both test cases presented in this section, TD bases have been employed for the polynomial approximations. The reason for this choice is that the error indicator (39) employed for the dimension-adaptive basis expansion fails to identify the elements that need further *h*- or *p*-refinement. This issue can be attributed to the high concentration of the posterior density, in combination with the greedy algorithm of the dimension-adaptive basis approach. Nevertheless, other sparse bases such as (non-adaptive) Smolyak sparse grids^{14,90} can be used instead. In that case, the benefits of using Leja nodes, in particular the ability to re-use existing nodes and corresponding model evaluations, remain valid.

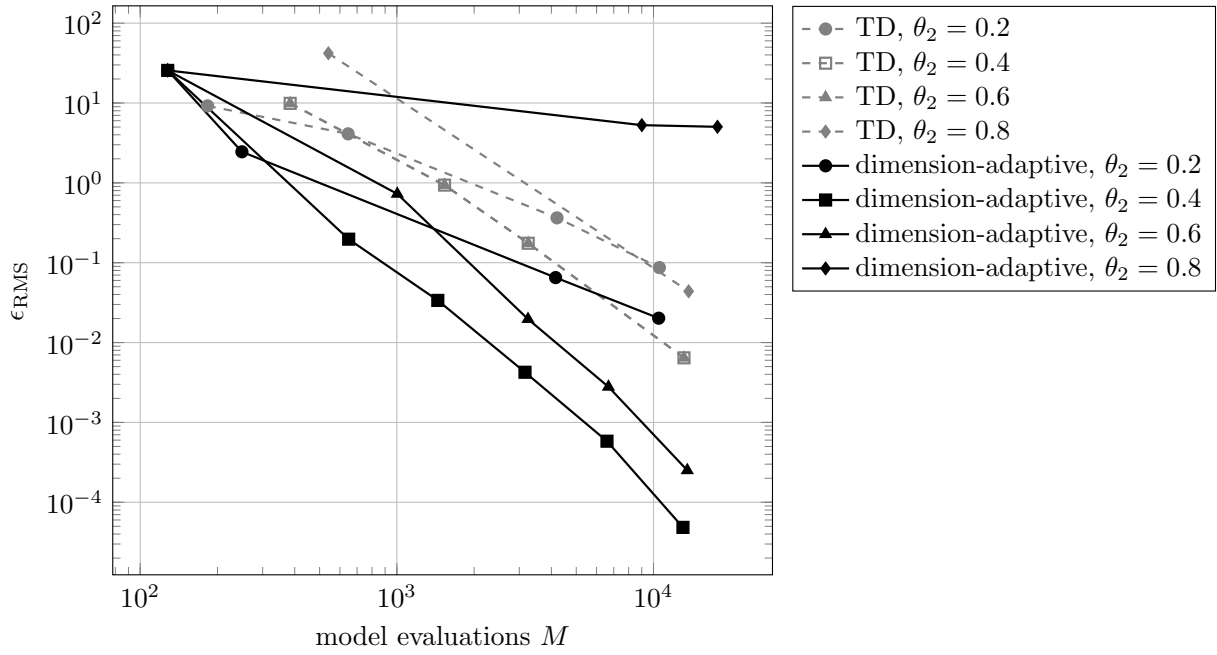


FIGURE 11 Convergence of the RMS error in dependence to model evaluations for the discontinuous Gentz function with 8 parameters.

5.2.3 | Multi-dimensional Gentz function

In the previous test case, the local polynomial expansions employ a TD basis. Although the TD basis is considered as a form of sparse approximation, in particular if compared to a tensor product basis approach, the computational costs related to the TD basis scale severely with the number of model parameters N . This is particularly true if h -refinement is additionally performed, since the complexity of the multi-element algorithm scales with $\mathcal{O}(2^N)$. Several strategies are available to delay the growth of the computational cost. In terms of Leja based collocations and the proposed information re-use, possible remedies are sparse grids⁹⁰ and dimension-adaptive strategies, as for example introduced in section 3. Here, we focus on the latter.

To showcase the capabilities of the hp -adaptive Leja collocation method combined with dimension-adaptivity, we revisit the discontinuous Gentz function, yet this time with a parameter vector of dimension $N = 8$. The function is given as

$$g(\mathbf{x}) = \begin{cases} 0, & \text{if } x_1 > u_1 \text{ and } x_2 > u_2, \\ \exp\left(\sum_{n=1}^8 a_n x_n\right), & \text{otherwise,} \end{cases} \quad (65)$$

with $u_1 = u_2 = 0.5$ and $a_n = 10 \cdot 2^{-n}$. The parameters x_n , $n = 1, \dots, 8$, are assumed to be uniformly distributed within $[0, 1]$. Note that the impact of each parameter x_n upon the model output is controlled through the constants a_n and is thus decreasing for increasing n . Due to this anisotropy, it is expected that the dimension-adaptive basis expansion strategy will be superior to an a priori chosen TD basis.

Figure 11 shows the RMS error in dependence to the model evaluations M , where both dimension-adaptive and TD bases have been employed. A parameter study for varying θ_2 is performed for both basis selection methods. The marks in Figure 11 show the results after convergence of the algorithm for different marking parameters θ_1 . Except for $\theta_2 = 0.8$, the dimension-adaptive bases outperform TD bases. In case of $\theta_2 = 0.8$, the local error indicator (39) for the dimension-adaptive approach is not capable of identifying the discontinuity of the Gentz function. However, in all other cases, a performance improvement of at least one order of magnitude is obtained when employing the dimension-adaptive basis expansion algorithm.

6 | CONCLUSION

In this work an hp -adaptive multi-element collocation method based on Leja nodes has been introduced. The presented method allows to re-use already computed model evaluations after h - or p -refinement. The local interpolation grids are stabilized after h -refinement by adding additional nodes and appropriately reordering the Leja sequence. To tackle the computationally demanding case of higher dimensional problems, a dimension-adaptive basis expansion algorithm has been employed. The work considered uniform as well as truncated normal distributed random inputs.

The numerical results showed that in the case of h -refinement, the proposed method is superior against approaches that do not utilize information re-use. The results also indicated that hp -adaptive refinement is to be preferred over pure h -refinement. Moreover, the proposed method was capable of approximating a highly concentrated posterior density in a two- and a four-dimensional inverse problem. Last, a test case featuring 8 input parameters demonstrated that higher dimensional problems can be tackled if dimension-adaptive bases are employed. It should however be noted that the proposed method is limited to low- and moderate-dimensional problems, due to the computational complexity of $\mathcal{O}(2^N)$ that accompanies h -refinement, where N denotes the number of parameters.

In summary, we may conclude that the proposed hp -adaptive collocation method based on Leja nodes is a reliable approach for surrogate modelling and UQ for functions with reduced regularity, as well as for functions featuring large gradients or sharp transitions. Further improvements in the convergence of the method are to be expected if the error indicator that is used to mark elements for further h - or p -refinement, is improved such that it is closer to the actual approximation error. To that end, possible solutions can be sought in the use of adjoint error indicators⁴⁷.

References

1. Matthies HG. Quantifying uncertainty: modern computational representation of probability and applications. In: Springer. 2007 (pp. 105–135).
2. Lee SH, Chen W. A comparative study of uncertainty propagation methods for black-box-type problems. *Structural and multidisciplinary optimization* 2009; 37(3): 239–253.
3. Bardsley JM. *Computational uncertainty quantification for inverse problems*. 19. SIAM . 2018.
4. Jiang P, Zhou Q, Shao X. *Surrogate model-based engineering design and optimization*. Springer . 2020.
5. Koziel S, Leifsson L. *Surrogate-based modeling and optimization*. Springer . 2013.
6. Tripathy RK, Bilionis I. Deep UQ: Learning deep neural network surrogate models for high dimensional uncertainty quantification. *Journal of computational physics* 2018; 375: 565–588.
7. Sacks J, Welch WJ, Mitchell TJ, Wynn HP. Design and analysis of computer experiments. *Statistical science* 1989; 4(4): 409–423.
8. Ghanem R, Spanos P. Polynomial Chaos in Stochastic Finite Elements. *Journal of Applied Mechanics* 1990; 57(1): 197.
9. Le Maître O, Knio O, Najm H, Ghanem R. Uncertainty propagation using Wiener–Haar expansions. *Journal of computational Physics* 2004; 197(1): 28–57.
10. Chouvion B, Sarrouy E. Development of error criteria for adaptive multi-element polynomial chaos approaches. *Mechanical Systems and Signal Processing* 2016; 66: 201–222.
11. Halder YV, Sanderse B, Koren B. An adaptive minimum spanning tree multielement method for uncertainty quantification of smooth and discontinuous responses. *SIAM Journal on Scientific Computing* 2019; 41(6): A3624–A3648.
12. Kawai S, Oyama A. Multi-Element Stochastic Galerkin Method Based on Edge Detection for Uncertainty Quantification of Discontinuous Responses. *Journal of Verification, Validation and Uncertainty Quantification* 2020; 5(4).
13. Wan X, Karniadakis GE. An adaptive multi-element generalized polynomial chaos method for stochastic differential equations. *Journal of Computational Physics* 2005; 209(2): 617–642.

14. Foo J, Wan X, Karniadakis GE. The multi-element probabilistic collocation method (ME-PCM): Error analysis and applications. *Journal of Computational Physics* 2008; 227(22): 9572–9595.
15. Agarwal N, Aluru NR. A domain adaptive stochastic collocation approach for analysis of MEMS under uncertainties. *Journal of Computational Physics* 2009; 228(20): 7662–7688.
16. Foo J, Karniadakis GE. Multi-element probabilistic collocation method in high dimensions. *Journal of Computational Physics* 2010; 229(5): 1536–1557.
17. Fuchs B, Gärcke J. Simplex Stochastic Collocation for Piecewise Smooth Functions with Kinks. *International Journal for Uncertainty Quantification* 2020; 10(1).
18. Jakeman JD, Narayan A, Xiu D. Minimal multi-element stochastic collocation for uncertainty quantification of discontinuous functions. *Journal of Computational Physics* 2013; 242: 790–808.
19. Ma X, Zabaras N. An adaptive hierarchical sparse grid collocation algorithm for the solution of stochastic differential equations. *Journal of Computational Physics* 2009; 228(8): 3084–3113.
20. Witteveen JA, Iaccarino G. Simplex stochastic collocation with ENO-type stencil selection for robust uncertainty quantification. *Journal of Computational Physics* 2013; 239: 1–21.
21. Ainsworth M, Oden JT. A posteriori error estimation in finite element analysis. *Computer methods in applied mechanics and engineering* 1997; 142(1-2): 1–88.
22. Ge L, Sun T. An adaptive hp-version stochastic Galerkin method for constrained optimal control problem governed by random reaction diffusion equations. *Computational and Applied Mathematics* 2022; 41(3): 1–30.
23. Narayan A, Jakeman JD. Adaptive Leja sparse grid constructions for stochastic collocation and high-dimensional approximation. *SIAM Journal on Scientific Computing* 2014; 36(6): A2952–A2983.
24. Chkifa A, Cohen A, Schwab C. High-dimensional adaptive sparse polynomial interpolation and applications to parametric PDEs. *Foundations of Computational Mathematics* 2014; 14(4): 601–633.
25. Loukrezis D, Römer U, De Gersem H. Assessing the performance of Leja and Clenshaw-Curtis collocation for computational electromagnetics with random input data. *International Journal for Uncertainty Quantification* 2019; 9(1).
26. Witteveen JA, Iaccarino G. Simplex stochastic collocation with random sampling and extrapolation for nonhypercube probability spaces. *SIAM Journal on Scientific Computing* 2012; 34(2): A814–A838.
27. Giovanis D, Shields M. Variance-based simplex stochastic collocation with model order reduction for high-dimensional systems. *International Journal for Numerical Methods in Engineering* 2019; 117(11): 1079–1116.
28. Babuška I, Nobile F, Tempone R. A stochastic collocation method for elliptic partial differential equations with random input data. *SIAM review* 2010; 52(2): 317–355.
29. Xiu D, Hesthaven JS. High-order collocation methods for differential equations with random inputs. *SIAM Journal on Scientific Computing* 2005; 27(3): 1118–1139.
30. Barthelmann V, Novak E, Ritter K. High dimensional polynomial interpolation on sparse grids. *Advances in Computational Mathematics* 2000; 12(4): 273–288.
31. Sudret B. Global sensitivity analysis using polynomial chaos expansions. *Reliability engineering & system safety* 2008; 93(7): 964–979.
32. Marzouk Y, Xiu D. A Stochastic Collocation Approach to Bayesian Inference in Inverse Problems. *Communications in Computational Physics* 2009; 6(4): 826–847.
33. Wagner PR, Marelli S, Sudret B. Bayesian model inversion using stochastic spectral embedding. *Journal of Computational Physics* 2021; 436: 110141.

34. Leja F. Sur certaines suites liées aux ensembles plans et leur application à la représentation conforme. *Annales Polonici Mathematici* 1957; 4(1): 8-13.

35. Bos LP, Caliari M. Application of modified Leja sequences to polynomial interpolation. *Dolomites Research Notes on Approximation* 2015; 8: 66-74.

36. Carnicer JM, Khiar Y, Peña JM. Central orderings for the Newton interpolation formula. *BIT Numerical Mathematics* 2019; 59(2): 371-386. doi: 10.1007/s10543-018-00743-2

37. Carnicer J, Khiar Y, Peña J. Optimal stability of the Lagrange formula and conditioning of the Newton formula. *Journal of Approximation Theory* 2017; 238. doi: 10.1016/j.jat.2017.07.005

38. Reichel L. Newton interpolation at Leja points. *BIT* 1990; 30(2): 332-346. doi: 10.1007/BF02017352

39. Calvi JP, Van MP. On the Lebesgue constant of Leja sequences for the unit disk and its applications to multivariate interpolation. *Journal of Approximation Theory* 2011; 163(5): 608-622.

40. Jantsch P, Webster CG, Zhang G. On the Lebesgue constant of weighted Leja points for Lagrange interpolation on unbounded domains. *IMA Journal of Numerical Analysis* 2019; 39(2): 1039-1057.

41. Taylor R, Totik V. Lebesgue constants for Leja points. *IMA Journal of Numerical Analysis* 2008; 30(2): 462-486. doi: 10.1093/imanum/drn082

42. Farcas IG, Latz J, Ullmann E, Neckel T, Bungartz HJ. Multilevel adaptive sparse Leja approximations for Bayesian inverse problems. *SIAM Journal on Scientific Computing* 2020; 42(1): A424-A451.

43. Jakeman JD, Franzelin F, Narayan A, Eldred M, Pltfüger D. Polynomial chaos expansions for dependent random variables. *Computer Methods in Applied Mechanics and Engineering* 2019; 351: 643-666.

44. Loukrezis D, De Gersem H. Approximation and Uncertainty Quantification of Systems with Arbitrary Parameter Distributions Using Weighted Leja Interpolation. *Algorithms* 2020; 13(3): 51.

45. van den Bos L, Sanderse B, Bierbooms W, Bussel vG. Bayesian Model Calibration with Interpolating Polynomials Based on Adaptively Weighted Leja Nodes. *Communications in Computational Physics* 2019; 27(1): 33-69.

46. Farcaş IG, Görler T, Bungartz HJ, Jenko F, Neckel T. Sensitivity-driven adaptive sparse stochastic approximations in plasma microinstability analysis. *Journal of Computational Physics* 2020; 410: 109394.

47. Georg N, Loukrezis D, Römer U, Schöps S. Enhanced adaptive surrogate models with applications in uncertainty quantification for nanolasers. *International Journal for Uncertainty Quantification* 2020; 10(2).

48. Nobile F, Tamellini L, Tempone R. Comparison of Clenshaw–Curtis and Leja quasi-optimal sparse grids for the approximation of random PDEs. In: Springer. 2015 (pp. 475-482).

49. Schillings C, Schwab C. Sparse, adaptive Smolyak quadratures for Bayesian inverse problems. *Inverse Problems* 2013; 29(6): 065011.

50. Clenshaw CW, Curtis AR. A method for numerical integration on an automatic computer. *Numerische Mathematik* 1960; 2(1): 197-205.

51. Gerstner T, Griebel M. Dimension–adaptive tensor–product quadrature. *Computing* 2003; 71(1): 65-87.

52. Gander W. Change of basis in polynomial interpolation. *Numerical linear algebra with applications* 2005; 12(8): 769-778.

53. Ghanem RG, Spanos PD. *Stochastic finite elements: a spectral approach*. Courier Corporation . 2003.

54. Xiu D, Karniadakis GE. The Wiener–Askey polynomial chaos for stochastic differential equations. *SIAM journal on scientific computing* 2002; 24(2): 619-644.

55. Feinberg J, Eck VG, Langtangen HP. Multivariate polynomial chaos expansions with dependent variables. *SIAM Journal on Scientific Computing* 2018; 40(1): A199–A223.
56. Soize C, Ghanem R. Physical systems with random uncertainties: chaos representations with arbitrary probability measure. *SIAM Journal on Scientific Computing* 2004; 26(2): 395–410.
57. Oladyshkin S, Nowak W. Data-driven uncertainty quantification using the arbitrary polynomial chaos expansion. *Reliability Engineering & System Safety* 2012; 106: 179–190.
58. Wan X, Karniadakis GE. Beyond Wiener–Askey expansions: handling arbitrary pdfs. *Journal of Scientific Computing* 2006; 27(1): 455–464.
59. Diaz P, Doostan A, Hampton J. Sparse polynomial chaos expansions via compressed sensing and D-optimal design. *Computer Methods in Applied Mechanics and Engineering* 2018; 336: 640–666.
60. Cheng K, Lu Z. Sparse polynomial chaos expansion based on D-MORPH regression. *Applied Mathematics and Computation* 2018; 323: 17–30.
61. Huan X, Safta C, Sargsyan K, et al. Compressive sensing with cross-validation and stop-sampling for sparse polynomial chaos expansions. *SIAM/ASA Journal on Uncertainty Quantification* 2018; 6(2): 907–936.
62. Peng J, Hampton J, Doostan A. A weighted ℓ_1 -minimization approach for sparse polynomial chaos expansions. *Journal of Computational Physics* 2014; 267: 92–111.
63. Tsilifis P, Huan X, Safta C, et al. Compressive sensing adaptation for polynomial chaos expansions. *Journal of Computational Physics* 2019; 380: 29–47.
64. Blatman G, Sudret B. Adaptive sparse polynomial chaos expansion based on least angle regression. *Journal of computational Physics* 2011; 230(6): 2345–2367.
65. Conrad PR, Marzouk YM. Adaptive Smolyak pseudospectral approximations. *SIAM Journal on Scientific Computing* 2013; 35(6): A2643–A2670.
66. Jakeman JD, Eldred MS, Sargsyan K. Enhancing ℓ_1 -minimization estimates of polynomial chaos expansions using basis selection. *Journal of Computational Physics* 2015; 289: 18–34.
67. Loukrezis D, Galetzka A, De Gersem H. Robust adaptive least squares polynomial chaos expansions in high-frequency applications. *International Journal of Numerical Modelling: Electronic Networks, Devices and Fields* 2020; 33(6): e2725.
68. Loukrezis D, De Gersem H. Adaptive sparse polynomial chaos expansions via Leja interpolation. *arXiv preprint arXiv:1911.08312* 2019.
69. Winokur J, Kim D, Bisetti F, Le Maître OP, Knio OM. Sparse pseudo spectral projection methods with directional adaptation for uncertainty quantification. *Journal of Scientific Computing* 2016; 68(2): 596–623.
70. Buzzard GT. Global sensitivity analysis using sparse grid interpolation and polynomial chaos. *Reliability Engineering & System Safety* 2012; 107: 82–89.
71. Buzzard GT. Efficient basis change for sparse-grid interpolating polynomials with application to T-cell sensitivity analysis. *Computational Biology Journal* 2013; 2013.
72. Porta G, Tamellini L, Lever V, Riva M. Inverse modeling of geochemical and mechanical compaction in sedimentary basins through polynomial chaos expansion. *Water Resources Research* 2014; 50(12): 9414–9431.
73. Saltelli A, Ratto M, Andres T, et al. *Global sensitivity analysis: the primer*. John Wiley & Sons . 2008.
74. Saltelli A, Annoni P, Azzini I, Campolongo F, Ratto M, Tarantola S. Variance based sensitivity analysis of model output. Design and estimator for the total sensitivity index. *Computer physics communications* 2010; 181(2): 259–270.

75. Sobol IM. Global sensitivity indices for nonlinear mathematical models and their Monte Carlo estimates. *Mathematics and computers in simulation* 2001; 55(1-3): 271–280.

76. Crestaux T, Le Maître O, Martinez JM. Polynomial chaos expansion for sensitivity analysis. *Reliability Engineering & System Safety* 2009; 94(7): 1161–1172.

77. Wan X, Karniadakis GE. Multi-element generalized polynomial chaos for arbitrary probability measures. *SIAM Journal on Scientific Computing* 2006; 28(3): 901–928.

78. Bürg M, Dörfler W. Convergence of an adaptive hp finite element strategy in higher space-dimensions. *Applied numerical mathematics* 2011; 61(11): 1132–1146.

79. Demkowicz L. *Computing with hp-adaptive finite elements: volume 1 one and two dimensional elliptic and Maxwell problems*. Chapman and Hall/CRC . 2006.

80. Dörfler W, Heuveline V. Convergence of an adaptive hp finite element strategy in one space dimension. *Applied numerical mathematics* 2007; 57(10): 1108–1124.

81. Houston P, Schwab C, Süli E. Discontinuous hp -finite element methods for advection-diffusion-reaction problems. *SIAM Journal on Numerical Analysis* 2002; 39(6): 2133–2163.

82. Mitchell WF, McClain MA. A comparison of hp -adaptive strategies for elliptic partial differential equations. *ACM Transactions on Mathematical Software (TOMS)* 2014; 41(1): 1–39.

83. Houston P, Süli E. A note on the design of hp-adaptive finite element methods for elliptic partial differential equations. *Computer Methods in Applied Mechanics and Engineering* 2005; 194(2-5): 229–243.

84. Nobile F, Tempone R. Analysis and implementation issues for the numerical approximation of parabolic equations with random coefficients. *International journal for numerical methods in engineering* 2009; 80(6-7): 979–1006.

85. Orszag SA, Bissonnette L. Dynamical Properties of Truncated Wiener-Hermite Expansions. *The Physics of Fluids* 1967; 10(12): 2603–2613.

86. Marelli S, Wagner PR, Lataniotis C, Sudret B. Stochastic Spectral Embedding. *International Journal for Uncertainty Quantification* 2020; 11. doi: 10.1615/Int.J.UncertaintyQuantification.2020034395

87. Boyd JP. *Chebyshev and Fourier Spectral Methods*. Courier Corporation . 2001.

88. Calvetti D, Somersalo E. Inverse problems: From regularization to Bayesian inference. *WIREs Computational Statistics* 2018; 10(3): e1427. doi: <https://doi.org/10.1002/wics.1427>

89. Bardsley JM. Computational Uncertainty Quantification for Inverse Problems. <https://github.com/bardsleyj/SIAMBookCodes>; 2018.

90. Smolyak S. Quadrature and interpolation formulas for tensor products of certain classes of functions. *Soviet Math. Dokl.* 1963; 4: 240–243.

